Comparison of functional thalamic segmentation from seed-based analysis and ICA

Hale, Joanne R.; Mayhew, Stephen D.; Mullinger, Karen; Wilson, Rebecca S.; Arvanitis, Theodoros N.; Francis, S.T.; Bagshaw, Andrew P.

DOI:
10.1016/j.neuroimage.2015.04.027

Document Version
Peer reviewed version

Citation for published version (Harvard):
Hale, JR, Mayhew, SD, Mullinger, K, Wilson, RS, Arvanitis, TN, Francis, ST & Bagshaw, AP 2015, 'Comparison of functional thalamic segmentation from seed-based analysis and ICA', *NeuroImage*, vol. 114, pp. 448-465. https://doi.org/10.1016/j.neuroimage.2015.04.027

Comparison of functional thalamic segmentation from seed-based analysis and ICA

Joanne R. Hale, Stephen D. Mayhew, Karen J. Mullinger, Rebecca S. Wilson, Theodoros N. Arvanitis, Susan T. Francis, Andrew P. Bagshaw

PII: S1053-8119(15)00317-1
DOI: doi: 10.1016/j.neuroimage.2015.04.027
Reference: YNIMG 12152

To appear in: *NeuroImage*

Received date: 19 December 2014
Accepted date: 7 April 2015

Please cite this article as: Hale, Joanne R., Mayhew, Stephen D., Mullinger, Karen J., Wilson, Rebecca S., Arvanitis, Theodoros N., Francis, Susan T., Bagshaw, Andrew P., Comparison of functional thalamic segmentation from seed-based analysis and ICA, *NeuroImage* (2015), doi: 10.1016/j.neuroimage.2015.04.027

Comparison of functional thalamic segmentation from seed-based analysis and ICA

Joanne R. Hale[1], Stephen D. Mayhew[1], Karen J. Mullinger[1,2], Rebecca S. Wilson[1],Theodoros N. Arvanitis[3], Susan T. Francis[2], Andrew P. Bagshaw[1]

[1]*School of Psychology, University of Birmingham, Birmingham, United Kingdom*
[2]*Sir Peter Mansfield Magnetic Resonance Centre, School of Physics and Astronomy, University of Nottingham, Nottingham, United Kingdom*
[3]*Institute of Digital Healthcare, WMG, University of Warwick, Coventry, United Kingdom*

Corresponding author:
Dr. Joanne Hale,
School of Psychology
University of Birmingham
Birmingham, B15 2TT
Tel : 0044 121 4143878
Email : j.hale.1@bham.ac.uk

ABSTRACT

Information flow between the thalamus and cerebral cortex is a crucial component of adaptive brain function, but the details of thalamocortical interactions in human subjects remain unclear. The principal aim of this study was to evaluate the agreement between functional thalamic network patterns, derived using seed-based connectivity analysis and independent component analysis (ICA) applied separately to resting state functional MRI (fMRI) data from 21 healthy participants. For the seed-based analysis, functional thalamic parcellation was achieved by computing functional connectivity (FC) between thalamic voxels and a set of pre-defined cortical regions. Thalamus-constrained ICA provided an alternative parcellation. Both FC analyses demonstrated plausible and comparable group-level thalamic subdivisions, in agreement with previous work. Quantitative assessment of the spatial overlap between FC thalamic segmentations, and comparison of each to a histological "gold-standard" thalamic atlas and a structurally-defined thalamic atlas, highlighted variations between them and, most notably, differences with both histological and structural results. Whilst deeper understanding of thalamocortical connectivity rests upon identification of features common to multiple non-invasive neuroimaging techniques (e.g. FC, structural connectivity and anatomical localisation of individual-specific nuclei), this work sheds further light on the functional organisation of the thalamus and the varying sensitivities of complementary analyses to resolve it.

Keywords: Functional Connectivity, Thalamocortical, Resting state, fMRI, ICA, Thalamus

1. Introduction

Most of the information we process about our external environment passes through the thalamus. Converging sensory information is consolidated by this fundamental sub-cortical structure, which also acts to regulate communication between extensive cortical areas (Alitto and Usrey, 2003; Saalmann, 2014; Sherman, 2007; Sherman and Guillery, 2002). The thalamus is composed of cytoarchitectonically distinct nuclei which either form connections to areas of cortex or act as transthalamic corticocortical connections, forming a dense thalamocortical network of complex bidirectional connections (Herrero et al., 2002; Mumford, 1998; Sherman and Guillery, 2013). Integration of neuronal activity across this thalamocortical network is believed to be vital for the maintenance of consciousness and mediation of the sleep/wake cycle (Bagshaw et al., 2014; Llinas, 2003), in addition to the processing of sensory and motor information (Alitto and Usrey, 2003). Due to the widespread influence of thalamocortical connections, disruptions of thalamic structure and function have been linked to numerous neuropsychiatric and neurological pathologies, including schizophrenia (Andreasen, 1997; Byne et al., 2009; Woodward et al., 2012), Parkinson's Disease (PD) (Henderson et al., 2000; Mak et al., 2014), chronic pain syndrome (CPS) (Gustin et al., 2011), epilepsy (Norden and Blumenfeld, 2002) and multiple sclerosis (MS) (Cifelli et al., 2002; Combarros et al., 1994). Furthermore, the implantation of deep brain stimulation (DBS) pacemakers into thalamic nuclei and/or thalamocortical pathways is used as a potential treatment for many of these disorders (epilepsy: Fisher, 2011; Ooi et al., 2011; movement disorders: Hubble et al., 1996; Putzke et al., 2005; Tourette Syndrome: Porta et al., 2009; chronic pain syndrome: Owen et al., 2006 and schizophrenia: Klein et al., 2013). The pressing basic scientific need to gain further insight into the role of the thalamus in the brain's complex network processing, as well as the clinical need to accurately locate relevant thalamic nuclei for DBS, has motivated research focused on delineating thalamic structure and connectivity.

Histology has largely formed the basis of knowledge on the structure and arrangement of thalamic nuclei (Morel et al., 1997), defining thalamic nuclei based on cyto- and myelo-architecture in stained slices of post-mortem tissue. Non-invasive exploration of the anatomy and the structural

connections of the thalamus has been facilitated by more recent work using diffusion-tensor imaging (DTI) (Behrens et al., 2003a; Johansen-Berg et al., 2005; Unrath et al., 2008; Wiegell et al., 2003; Zhang et al., 2010). Behrens and colleagues (2003) used probabilistic diffusion tractography to map white-matter fibre pathways between each voxel in the thalamus and a set of *a priori* defined cortical regions of interest (ROIs). Allocating each thalamic voxel to the cortical area to which it was most strongly connected revealed a map of thalamic clusters, likened to thalamic nuclei or subgroups of nuclei identified from histology (Johansen-Berg et al., 2005).

Whilst structural connectivity (SC) refers to a direct anatomical connection, functional connectivity (FC) is defined as a statistical interdependency between the timecourses recorded from disparate brain regions (Friston, 1994). Measures of FC and SC have been shown to be complementary, however a functional association between regions does not necessarily reflect structural links (Greicius et al., 2009; Honey et al., 2009; Koch et al., 2002; Vincent et al., 2007), suggesting that FC warrants independent study. FC, assessed by correlations between low frequency (<0.1 Hz) Blood Oxygenation Level-Dependent (BOLD) functional MRI (fMRI) signals, has been previously reported between wide-ranging cortical areas. The realisation that cortical regions display FC in the absence of a specific task (Biswal et al., 1995) led to a rapid growth in the study of the brain's intrinsic activity (Cordes et al., 2000; De Luca et al., 2006; Greicius et al., 2003; Gusnard and Raichle, 2001; Lowe et al., 1998; Raichle et al., 2001) (for reviews see: Fox and Raichle, 2007 and Van Dijk et al., 2010), with a series of resting state functional networks having been identified, which are comparable to those observed during performance of task-based paradigms (Smith et al., 2009).

Whilst a large body of neuroimaging research has studied functional network activity between cortical regions, few studies have explicitly considered subcortical connections. Zhang and colleagues (2008) studied FC between the cortex and the thalamus using seed-based fMRI analysis, computing the partial correlation between cortical ROIs and each voxel in the thalamus. The resulting spatially distinct patterns of thalamocortical FC largely resembled structural connections, as measured using DTI, and were similar to those from histology (Zhang et al., 2010). Using the same

approach Woodward et al. (2012) revealed consistent thalamocortical FC maps in healthy participants, but found that in patients with schizophrenia a smaller region of the thalamus was functionally connected to the prefrontal cortex and a larger area of the thalamus was functionally connected to the sensorimotor cortex compared with a cohort of healthy controls. Independent component analysis (ICA), a multi-variate, data-driven approach to FC analysis, has recently been used to isolate subunits of the basal ganglia and thalamus (Kim et al., 2013). Whilst the similarity of FC, assessed using seed-based analysis and ICA, has been considered for cortical networks (Rosazza et al., 2012; Van Dijk et al., 2010), a direct comparison of thalamic parcellations, generated using these two methodologies, is yet to be considered, nor has the related question of their relative agreement with a standardised thalamic atlas (Morel et al., 1997).

In this work, we apply seed-based partial correlation FC analysis and group ICA (GICA) to resting state fMRI data to non-invasively segment the human thalamus, based on FC. We aim to compute the spatial correspondence in group FC maps of the thalamus between each analysis technique, and perform a quantitative comparison with a histological thalamic atlas (Krauth et al., 2010; Morel et al., 1997) and with the structurally-defined Oxford thalamic atlas (Behrens et al., 2003a, 2003b). Whilst the majority of previous thalamic segmentation studies have been performed at the group-level, it is expected that individual differences in thalamic organisation will be present (Burgel et al., 2006; Rademacher et al., 2002), which may be linked to differences in behavioural performance (Baldassarre et al., 2012; Mueller et al., 2013). A secondary aim is therefore to consider the relationship between thalamocortical maps of individual participants derived from seed-based analysis and ICA, while investigating whether the same variation in FC measures is captured by both analyses.

2. Methods

2.1. Participants

21 healthy volunteers (10 male, 25±3 years) took part in the study which was approved by the Research Ethics Board of the University of Birmingham. Participants had no history of neurological

disorders, neuropsychiatric disorders or sleep disorders. All participants gave written, informed consent.

2.2. MR Data acquisition

Participants underwent a 15 minute resting state experiment during which they were asked to lie still and relaxed in the MR scanner, whilst keeping their eyes open. All participants reported that they remained awake for the scan duration. fMRI data were acquired using a 3 Tesla Philips Achieva MR scanner (Philips, Netherlands) with a body transmit coil and a 32 channel SENSE receive head coil. BOLD gradient-echo echo planar imaging (GE-EPI) data were acquired with the following parameters: TE = 34 ms; spatial resolution = 3 x 3 x 4 mm^3; field of view = 240 x 128 x 240 mm; flip angle = 80^0; SENSE factor 2; TR = 2 s for 32 slices; 450 dynamics. Respiratory and cardiac fluctuations were recorded, using a pneumatic belt around the upper abdomen and a vectorcardiogram respectively, to facilitate correction of physiological noise. A high resolution (1 mm isotropic), T_1-weighted, anatomical image was also acquired for each participant to enable co-registration of individual data to MNI space (MPRAGE image acquisition parameters: TR =8.4ms; TE=3.8ms; field of view = 232 x 288 x 175 mm; flip angle =8^0).

2.3. Pre-processing

All fMRI data were pre-processed using FSL (FMRIB Software Library, http://www.fmrib.ox.ac.uk/fsl, Smith et al., 2004) and custom written software in Matlab (MathWorks, Natick, USA). Preprocessing steps included automated brain extraction using BET (Smith, 2002), motion correction using MCFLIRT, physiological noise correction using RETROICOR (Glover et al., 2000), slice timing correction, spatial smoothing using a Gaussian kernel (FWHM = 4 mm) and high-pass temporal filtering (> 0.01 Hz). Motion parameters, white matter and cerebral spinal fluid (CSF) signals were removed from each voxel by linear regression, and all data were co-registered to the standard 2 mm isotropic MNI space using FLIRT in FSL. Co-registration was performed in two steps: subject's EPI data were initially co-registered to their brain extracted high-resolution anatomical image; the

anatomical image was then co-registered to the MNI brain and the transform applied to the co-registered EPI data.

2.4. Cortical ROI definition

In line with previous thalamic segmentation studies (Behrens et al., 2003a; Zhang et al., 2008; Zhang et al., 2010), we divided the cortex into a number of functionally homologous regions previously shown to be connected to disparate areas of the thalamus. Five cortical ROIs were defined in standard MNI space by combining masks from the Harvard-Oxford cortical atlas (http://fsl.fmrib.ox.ac.uk/fsl/fslwiki/Atlases, Desikan et al., 2006; Frazier et al., 2005; Goldstein et al., 2007; Makris et al., 2006) in FSL: 1) 'Occipital and Parietal': including angular gyrus, cingulate gyrus, cuneal cortex, intracalcarine cortex, lateral occipital cortex, occipital fusiform gyrus, temporal occipital fusiform cortex, supracalcarine cortex, supramarginal cortex, parietal operculum, precuneus cortex, and the occipital pole; 2) 'Motor and Premotor': consisting of precentral gyrus and supplementary motor area; 3) 'Somatosensory': consisting of postcentral gyrus; 4) 'Prefrontal': consisting of anterior cingulate gyrus, frontal operculum cortex, frontal pole and inferior, middle and superior frontal gyri and paracingulate gyrus; and 5) 'Temporal': consisting of Heschl's gyrus, inferior, middle and superior temporal gyri, parahippocampal gyrus, planum polare, planum temporale, parahippocampal gyrus, temporal fusiform cortex and temporal pole. A thalamus ROI was defined from the Oxford thalamic connectivity atlas (http://fsl.fmrib.ox.ac.uk/fsl/fslwiki/Atlases, Behrens et al., 2003a, 2003b) thresholded at a probability of 25%, chosen to ensure that the whole thalamus was included (Serra et al., 2013). Figure 1 shows the five cortical ROI masks and the thalamus ROI mask overlaid on the MNI brain.

2.5. Seed-based FC analysis

For the seed-based FC analysis, partial correlation was computed between BOLD timecourses, extracted from each thalamic voxel and the mean BOLD timecourse from each cortical ROI. Partial correlation was computed between the thalamus and each cortical ROI, whilst controlling for the influence of the other cortical ROI timecourses. Previous work has shown that partial correlation is

more similar to effective measures of connectivity (Marrelec et al., 2006) and demonstrates increased sensitivity for identifying network connectivity (Smith et al., 2011) than Pearson correlation. In this work, partial correlation was used to estimate direct connections between thalamic voxels and cortical ROIs.

Partial correlation maps for each cortical ROI were converted to Z-score images, by applying Fisher's r-to-z transform and assuming the number of effective degrees of freedom, n, was equal to the number of dynamics, N, divided by the Bartlett correction factor (BCF) (Fox et al., 2005; Zhang et al., 2008). The Bartlett correction factor was applied to account for the temporal autocorrelation in BOLD timecourses and was computed from the integral across time of the squared autocorrelation function for each participant (BCF=1.92±0.03, mean±standard error across participants). Individual Z-score maps were combined across participants using a random-effects analysis.

To summarise group-level seed-based results a winner-take-all (WTA) map was generated in which each thalamic voxel was assigned to a cortical ROI based on the highest positive partial correlation value. In addition, to enable visualisation of individual thalamocortical FC patterns, WTA maps were also generated for each subject. The percentage of thalamic voxels in each WTA map assigned to each cortical ROI was calculated for each subject and then averaged across subjects.

2.6. Independent Component Analysis (ICA)

As an alternative to seed-based FC analysis and to allow more flexibility in sub-dividing the thalamus, ICA was used to decompose fMRI data from the thalamus alone into spatially independent maps and associated timeseries. The thalamus ROI (Figure 1B) was used to mask the pre-processed resting state fMRI data. Only thalamic voxels were then entered into a group-level independent component analysis (GICA), using the temporal concatenation option of MELODIC (Beckmann and Smith, 2004) in FSL. To consider the effect of dimensionality on ICA thalamic parcellation, ICA was separately run with 10 or 20 components (ICs). Using MELODIC, the data were first whitened and then principal component analysis (PCA) was applied to perform the dimensionality reduction, this retained 48% of the subject variance for the 10 component PCA and 60% of the variance for the 20 component PCA.

In addition fMRI data from just the right or left thalamus were selected and each decomposed with separate GICAs in order to investigate the bilateral nature and reproducibility of thalamic components. Note for the single hemisphere GICAs, for 10 components 54% of the variance was kept following PCA **(consistently for both left and right hemisphere data)**, and 68% for the 20 component PCA **(for both left and right hemisphere data)**.

Dual regression (Beckmann et al., 2009; Filippini et al., 2009) was then applied to the group-level results in order to generate subject-specific versions of the thalamic spatial maps and their associated timeseries. First, for each subject, the group-average spatial maps were regressed (as spatial regressors in a multiple regression) onto the subject's 4D space-time fMRI dataset. This resulted in a set of subject-specific timeseries, one per group-level spatial map. Next, those timeseries were regressed (as temporal regressors, again in a multiple regression) onto the same 4D dataset, resulting in a set of subject-specific spatial maps, one per group-level spatial map.

2.6.1. WTA maps for ICs

For each IC timecourse in each individual participant, the partial correlation was computed with the mean timeseries from each of the five cortical ROIs. These correlation coefficients were averaged across participants and used to generate a group-level WTA map. Each thalamic voxel was assigned to one IC based on its maximum Z-score in each IC, selecting the voxels most strongly related to each of the ICs. Each IC was then colour-coded, based on the maximal average partial correlation across subjects to each of the cortical ROIs. WTA maps were also generated for individual participants using individual spatial maps outputted from the dual regression analysis. The percentage of thalamic voxels in each WTA map assigned to each cortical ROI was calculated and then averaged across subjects.

2.7. Calculating spatial overlap

We quantitatively assess**ed** the spatial similarity between the seed-based analysis and GICA functional thalamic segmentations as well as with histological and structural connectivity results. Dice's coefficient measures the similarity or volume overlap between two binary images and is

calculated as: the ratio of twice the number of non-zero voxels common to both images divided by the total number of non-zero voxels in each image. For perfect correspondence the Dice's coefficient is 1, while a coefficient of 0 corresponds to no overlap. To facilitate normalisation of volume differences across pairs of 2D image slices, we applied the generalized Dice's coefficient, whereby a weighting parameter (α_i) for each slice i, is introduced as follows (Crum et al., 2006):

$$\mathrm{DC}_{\mathrm{generalized}} = \frac{2\ \sum_{i=1}^{n} \alpha_i\ \mathrm{N}(|\mathrm{A_i} \cap \mathrm{B_i}|)}{\sum_{i=1}^{n} \alpha_i\ \mathrm{N}(|\mathrm{A_i}|) + \mathrm{N}(|\mathrm{B_i}|)}$$

We used two weightings, $\alpha_i=1$ which is the standard Dice coefficient, and $\alpha_i=1/V_i$ where V_i is the mean volume ($V_i=N(|A_i|)+N(|B_i|)/2$), thereby normalising volumes across slice pairs. All figures were generated with $\alpha_i=1/V_i$, but supplementary tables show the equivalent values for $\alpha_i=1$.

The group-level ICA and seed-based maps were thresholded (seed-based extent threshold corresponding to $p < 0.001$ and ICA components threshold corresponding to alternative hypothesis threshold of $P > 0.5$), yielding binary images and generalized Dice coefficients were computed for each pair of slices.

To compare the spatial overlap to previous histological results from a digital stereotactic thalamic atlas (Krauth et al., 2010; Morel et al., 1997), generalized Dice's coefficient was separately applied to the group-level seed-based and GICA results. Note that the high-resolution thalamic atlas (1mm isotropic resolution) was first downsampled to 2-mm spatial resolution to match the functional parcellation results.

In addition, to compare our functional parcellations with the Oxford thalamic connectivity atlas derived using DTI (http://fsl.fmrib.ox.ac.uk/fsl/fslwiki/Atlases, Behrens et al., 2003a, 2003b), we similarly employed generalized Dice's coefficient separately to the group-level seed-based and GICA results. The probabilistic Oxford thalamic connectivity atlas masks thresholded at a probability of 25% were used and in-line with our seed-based methodology, Oxford atlas masks of thalamic regions connected to Occipital and Parietal regions were combined into a single mask as well as the Motor and Premotor masks, resulting in 5 Oxford thalamic atlas masks.

3. Results

3.1. Group-level results

3.1.1. Seed-based analysis

The group-level thalamocortical connectivity maps for each of the five cortical ROIs are shown in Figure 2. We observed that bilateral symmetric clusters of thalamic voxels were functionally connected to specific cortical ROIs. The 'Occipital and Parietal' ROI was found to be connected to the largest area of the thalamus, and whilst the variance in the cortical timecourses was similar and therefore not thought to be driving the high 'Occipital and Parietal' connectivity, this could in part be explained by the 'Occipital and Parietal' being the largest ROI (Table 1). From comparison with the Krauth/Morel thalamic atlas (see also Figure 8A), the 'Occipital and Parietal' ROI exhibited the strongest FC with the lateral geniculate nuclei (DC = 0.07) and inferior pulvinar (DC = 0.08), and lesser FC with medial geniculate nuclei (DC = 0.06), lateral and medial parts of the pulvinar (DC = 0.02) with some extension into part of the right mediodorsal nucleus. The 'Motor and Premotor' ROI was functionally connected to ventral posterior medial nuclei (DC = 0.1), ventral lateral posterior nuclei (DC = 0.14), the ventral posterior lateral nuclei (DC = 0.11) and the centre median nuclei. The 'Somatosensory' ROI displayed consistent FC across the subject group with only the anterior portion of the pulvinar and ventral posterior nuclei (DC = 0.01). Connections to the 'Prefrontal' ROI were seen to overlap with the mediodorsal (DC = 0.15) and ventral anterior nuclei (DC = 0.15), with connections with right thalamic nuclei being higher than to left. Finally, the 'Temporal' ROI was shown to be functionally connected with the medial geniculate nuclei (DC = 0.13) and portions of the pulvinar (DC = 0.02). Note that here, the term 'nuclei' is used to describe bilateral thalamic subregions. Results presented here are in general agreement with anatomical segmentations of the thalamus from previous histological post-mortem work in humans (Morel et al., 1997) and primates (Jones, 1998), as well as non-invasive human structural (Behrens et al., 2003a; Johansen-Berg et al., 2005; Zhang et al., 2010) and functional connectivity (Woodward et al., 2012; Zhang et al., 2008, 2010) studies. A full quantitative comparison of seed-based results with those from GICA, histology and the Oxford thalamic atlas is given in sections 3.1.3., 3.1.4. and 3.1.5. respectively.

Since the interpretation of negative correlations remains somewhat contentious (Fox et al., 2009; Murphy et al., 2009; Weissenbacher et al., 2009), especially when using partial correlations (Birn et al., 2006; Smith et al., 2012; Zhang et al., 2008), only positive correlations are shown in Figure 2. For completeness, Figure S1 shows both positive and negative group-level partial correlation maps. To ensure that our results were not driven by spatial smoothing, we also repeated the seed-based analysis without applying any smoothing and found that results were largely unchanged (Figure S2).

Table 1. Number of voxels in each cortical ROI and the average standard deviation of ROI timecourses with standard error across participants shown

Cortical ROI	Number of voxels in ROI	Average standard deviation of ROI timecourse ± standard error across participants
'Occipital and Parietal'	64,842	36 ± 2
'Motor and Premotor'	20,967	38 ± 3
'Somatosensory'	15,438	38 ± 3
'Prefrontal'	53,714	27 ± 2
'Temporal'	38,647	26 ± 2

The group-level seed-based WTA map is shown in Figure 6A. Inferior regions of the thalamus, i.e. the lateral geniculate nuclei and medial geniculate nuclei, were assigned to the 'Occipital and Parietal' and 'Temporal' ROIs, and the mediodorsal nuclei (especially the right mediodorsal nucleus) was assigned to the 'Prefrontal' ROI, as would be expected from histology. Meanwhile, the 'Motor and Premotor' ROI was assigned to voxels covering ventral posterior lateral nuclei, which are thought to project to Somatosensory cortices, whilst only a few posterior voxels at the edge of the thalamus were assigned to the 'Somatosensory' ROI. As predicted from the seed-based maps (Figure 2) it should also be noted that assignment to the 'Occipital and Parietal' ROI showed widespread dominance, particularly in more superior slices.

3.1.2. Independent Component Analysis

Figures 3 and 4 show the effect of dimensionality on GICA thalamic parcellation using both 10 and 20 components respectively. In general, and for both dimensionalities, GICA resulted in bilateral and

symmetrical ICs, covering physiologically plausible regions of the thalamus. For GICA with 10 components, only IC7 was shown to be lateralised. Several components resemble individual thalamic nuclei. For example, IC1 overlaps with the geniculate nuclei (lateral and medial) (DC = 0.06, DC = 0.16), IC2 overlaps with the lateral pulvinar (DC = 0.07), IC3 shows the anterior medial nuclei and to a lesser extent the ventral anterior nuclei (DC = 0.21), IC5 resembles the mediodorsal nuclei (DC = 0.38), IC7 right pulvinar (DC = 0.05, left and right pulvinar) and IC10 the ventral posterior lateral nuclei (DC = 0.16). Further details of the quantitative comparison of these overlaps, in terms of Dice's coefficients in relation to the histological atlas, are to be found in section 3.1.4. For the 20 component GICA, results were found to be largely similar to those of the 10 component analysis, suggesting reproducible patterns of components across dimensionality. Whilst more than half of the components for the 20 dimension GICA were bilateral, 7/20 components were lateralised predominantly to the left thalamic hemisphere. This suggests that the main effect of increasing the dimensionality was to split previously bilateral components into unilateral regions.

Figure 5 shows the GICA thalamic parcellations for the left (red) and right (blue) hemispheres separately, each with a dimensionality of 10. ICs derived from the right hemisphere data analysis are displayed alongside those with the closest spatial match from the left hemisphere analysis. For all left hemisphere ICs, apart from IC10, spatially corresponding ICs were generated from the right hemisphere analysis. Results of running GICA separately for the two hemispheres with 20 dimensions (see supplementary Figure S3) were found to be very similar. The expression of similar spatial patterns of ICs when GICA was separately performed on left and right thalamus data suggests that the bilateral pattern of ICs generated from the whole thalamus GICA was reliable, and not a random or artifactual outcome of the ICA process.

After parcellating the thalamus using GICA, the correlation was computed between the timecourse of each IC and the timecourse of each cortical ROI to establish the functional specificity of each of the ICs. The group-level WTA maps in Figure 6B show each of the 10 and 20 components colour-coded based on the maximum partial correlation with each of the cortical ROIs. For the two GICA

dimensionalities, group-level WTA maps were found to be generally comparable with maximal correlations with cortical ROIs found to cluster in similar regions of the thalamus, although there is some suggestion of differences, which suggests that increasing the dimensionality has also had an effect on the pattern of thalamocortical FC. The 'Motor and Premotor' cortical timecourse was found to be maximally functionally connected to ICs overlapping ventral posterior lateral and ventral posterior medial nuclei and ventral lateral nuclei; in agreement with the group-level seed-based 'Motor and Premotor' correlation map (Figure 2), but in contrast to the seed-based WTA map (Figure 6A). ICs occupying anterior medial nuclei and mediodorsal nuclei (especially the right mediodorsal nucleus) were found to be most highly correlated with the 'Prefrontal' ROI, also in agreement with the seed-based correlation results and WTA map. The 'Temporal' ROI was found to be most correlated with the component overlapping both bilateral medial geniculate nuclei and lateral geniculate nuclei, as well as bilateral pulvinar. WTA results for the 'Occipital and Parietal' and 'Somatosensory' ROIs showed the biggest deviations from seed-based connectivity results. Both the GICA and seed-based WTA maps showed that the 'Occipital and Parietal' ROI was maximally correlated with the pulvinar but also displayed a generally more widespread connectivity pattern (particularly the 20 component results), but unlike the seed-based WTA map, in the GICA WTA maps the 'Occipital and Parietal' ROI was not found to be connected to the lateral geniculate nuclei. Meanwhile connections with the 'Somatosensory' ROI were more prominent in the GICA WTA maps (occurring along central midline nuclei) than in the group-level seed-based WTA map.

3.1.3. Spatial comparison of seed-based analysis and whole thalamus GICA results

To facilitate a quantitative spatial comparison between group-level seed-based connectivity results and whole thalamus GICA, the generalized Dice's coefficient computed across slices was measured between GICA maps derived with 10 components and group-level seed-based connectivity maps for each cortical ROI (Figure 7). Generally each of the IC maps had substantial overlap with at least one of the seed-based cortical connectivity maps. While some component maps (IC7, IC10) clearly had maximal overlap with a single cortical map, others are similarly correlated with two (IC1, IC2, IC3,

IC5, IC6, IC8) or more (IC4, IC9) cortical maps. In the case of IC1, this is due to the component overlapping with both the lateral and the medial geniculate nuclei, which are prominent regions of both the 'Occipital and Parietal' and 'Temporal' seed-based maps, respectively. IC3 was found to mainly overlap with the 'Prefrontal' seed-based connectivity map (which has foci in the right mediodorsal and ventral anterior nuclei). However, IC3 also overlapped with the 'Occipital and Parietal' seed-based map since it also showed correlations with the right mediodorsal nucleus. Overall, there was a degree of specificity that allowed the predominant cortical connectivity of each of the IC maps to be identified, plus substantial overlap between the GICA and specific seed-based results. Similar conclusions can be drawn from the 20 components maps (Figure S4). Tables showing the breakdown of generalized Dice coefficient calculations for computing the overlap between the two functional parcellations are shown in Table S1.

3.1.4. Spatial comparison of seed-based analysis and GICA results and histology

Figure 8B shows the generalized Dice's coefficient over slices, measured between each seed-based FC map and selected Morel-defined thalamic nuclei from the Krauth atlas (Figure 8A). In the digitized version of the Morel atlas, Krauth et al. (2010) include 52 subdivisions of the thalamus; for clarity here we show overlap with only a subset of these nuclei selected based on previously reported thalamocortical projections (Krebs et al., 2012; Sherman and Guillery, 2013).

Of all of the group seed-based connectivity maps, the only one to show a clear overlap with a single thalamic nucleus was the 'Temporal' FC map, which overlapped with right and left medial geniculate nuclei, structures which are believed to primarily project to auditory cortex. The 'Prefrontal' map overlapped with the posterior part of mediodorsal nuclei, which is thought to be structurally connected to prefrontal cortex, but it also with the ventral nuclei, which are considered to be primarily structurally connected to motor and somatosensory cortices. Similarly, the 'Occipital and Parietal' map overlaid with the lateral geniculate nuclei and pulvinar (nuclei which are associated with visual processing) but also overlapped equally highly with a number of other thalamic nuclei. Ventral (in particularly ventral lateral) nuclei, thought to structurally connect to somatosensory as

well as motor cortex, were found here to overlap with the 'Motor and Premotor' map. The 'Somatosensory' map had low overlap with all histological nuclei; however, this is perhaps to be expected due to the small spatial extent of the group-level 'Somatosensory' seed-based map and histological subunits.

Figure 8C displays the generalized Dice's coefficient measured between the same selected histological nuclei and the 10 component GICA results. Compared with the seed-based vs. Morel overlap results (Figure 8B), the GICA results appear to reveal more specific thalamic nuclei, i.e. a majority of components were found to overlap with a single histological nucleus or functional subgroup of nuclei, although this may be driven by the relatively large cortical regions used for the seed-based analysis. Components overlapped distinctly with nuclei which are associated with 4 out of the 5 cortical ROIs for the 10 component GICA. For example, IC1 overlapped substantially with the medial geniculate nuclei (associated with temporal cortex), IC2 with the lateral pulvinar (associated with visual cortex), IC3 overlapped with ventral anterior and lateral nuclei (associated with motor cortex), whilst IC5 and IC8 were seen to overlap substantially with mediodorsal nuclei (associated with prefrontal cortex). No components overlapped solely with the ventral posterior nuclei (thought to be connected to somatosensory cortex). Many of the remaining components showed more widespread overlap with Morel nuclei, in particular IC10 and to a lesser extent IC7. Results for the 20 component GICA are shown in Figure S5 and are largely similar to those discussed here for 10 components.

Supplementary tables showing the breakdown of generalized Dice coefficient calculations between each functional parcellation and the histological atlas (Tables S2 and S3) reveal that the functional parcellations extend over many more voxels than the Morel atlas nuclei and that this difference in volumes contributes to, although is not solely responsible for, the generally low overlap values observed between the functional results and histology.

3.1.5. Spatial comparison of seed-based analysis and GICA results and structural connectivity

The measured overlaps between the group seed-based and GICA thalamic maps with the Oxford thalamic atlas (Figure 9A) are shown in Figures 9B and 9C. 'Occipital and Parietal', 'Motor and Premotor' and 'Prefrontal' seed-based maps showed the highest overlap with the corresponding Oxford thalamic atlas maps (DC = 0.4; DC = 0.18 and DC = 0.6, respectively) (Figure 9B). Meanwhile, whilst the 'Temporal' seed-based map overlapped with a single Oxford atlas map, it was also shown to correspond to the Oxford thalamic regions connected to Occipital and Parietal cortices (DC = 0.44). This discrepancy may in part be due to the Oxford atlas map assigned to Occipital and Parietal cortices extending over both the lateral and medial geniculate nuclei (which have been shown to project to visual and auditory cortices, respectively). The 'Somatosensory' seed-based map in comparison displayed equivalent overlap with three Oxford atlas maps, including that assigned to Somatosensory cortex, but it should be noted that all Dice coefficients were low (<0.1).

Figure 9C displays the generalized Dice's coefficient between the Oxford thalamic atlas maps and the 10 component GICA results. A number of components demonstrated overlap with a single Oxford atlas map; IC1 showed maximal overlap with the Occipital and Parietal Oxford map (DC = 0.6), IC2 and IC8 with the Temporal Oxford atlas map (DC = 0.38 and DC = 0.41), IC3 and IC4 with the Prefrontal Oxford atlas map (DC = 0.42 and DC = 0.71). Other components overlapped equally highly with two (IC5, IC6, IC9 and IC10) or more (IC7) Oxford atlas maps. Results of the comparison between the 20 component GICA results and Oxford thalamic atlas is shown in Figure S6 and are similar to those for the 10 components, except that some of the 20 ICs overlapped maximally with the Motor and Premotor Oxford atlas maps (IC4 and IC5). No components for either GICA dimensionalities were found to overlap with the Somatosensory Oxford atlas map.

Tables showing the breakdown of Dice coefficient calculations comparing functional parcellations with the Oxford thalamic atlas are shown in Tables S4 and S5.

3.2. Assessing inter-subject spatial variability

In addition to assessing group-level results, we also compared the two analysis techniques in terms of their sensitivity to individual variations in thalamocortical FC patterns. The WTA maps shown in Figure 10A were generated to summarise seed-based and GICA FC results for individual participants. For both analyses, considerable inter-subject variability was observed in the WTA maps for both seed-based and ICA methods. For the seed-based analysis the 'Occipital and Parietal' ROI was found to connect with the largest area of the thalamus across subjects (Figures 10B and 10C), but also showed greatest inter-individual variability (e.g. Fig 10A, left hand images of Participant 1 compared with Participant 17). WTA maps for both 10 and 20 component GICA displayed variability across participants (Figure 10A, right hand images and Figure S7), with some additional variability observed within participants for the two GICA dimensionalities, suggesting that as well as lateralising ICs, increasing GICA dimensionality changed which cortical ROI some ICs were most functionally connected to. In addition, GICA WTA maps from either dimensionality were not consistently equivalent to those from the seed-based analysis.

4. Discussion

Here, we apply two commonly used methodologies, namely seed-based analysis and GICA, to parcellate the human thalamus in resting state fMRI data. Our findings provide a novel comparison of the application and utility of these techniques for assessing subcortical connectivity, extending previous work and providing further evidence that the two analysis techniques are able to reveal functional subunits of the thalamus. Even though similarities were observed, thalamocortical FC results from seed-based connectivity analysis and GICA displayed notable differences at both the group and individual subject level. Overlap between FC-based methods and a histological atlas showed some additional specificity provided by the GICA approach, whereby component maps tended to be more prominently connected to single histological nuclei or functionally connected group of nuclei. Use of GICA with data from left and right thalami separately identified a high degree

of bilateral symmetry, confirming previous histological reports that the nuclei are largely symmetrical (Eidelberg and Galaburda, 1982).

4.1. Group-level seed-based analysis and ICA

Seed-based analysis and GICA have been extensively applied to measure the FC of numerous resting state cortical networks (seed-based analysis: Biswal et al., 1995; Fox et al., 2005; Greicius et al., 2003; ICA: Beckmann et al., 2005; Beckmann et al., 2009; Kiviniemi et al., 2003; Kiviniemi et al., 2009) and more recently independently used to identify thalamic segmentations (Kim et al., 2013; Zhang et al., 2008; Zhang et al., 2010). Combining results at the group level we reveal largely bilateral and distinct groups of thalamic voxels displaying consistently high FC with each of the five cortical regions investigated (Figure 2). The locations of these clusters are largely in agreement with those previously identified using seed-based analysis (Zhang et al., 2008, 2010; Woodward et al., 2012). GICA constrained to thalamic voxels (similarly to Kim et al., 2013) was used to decompose data from the thalamus into sets of 10 and 20 independent spatial maps (Figures 3 and 4, respectively). The majority of the maps showed bilateral clusters of thalamic voxels each occupying distinct areas of the thalamus. Furthermore, upon visual inspection a number of the ICs could plausibly be thought to represent individual thalamic nuclei. Analogous subregions of the thalamus to those reported here were also preferentially observed in Kim et al. (2013).

4.2. Comparison of group-level seed-based analysis and GICA results

Whilst previous studies have used either a seed-based analysis or GICA to study thalamocortical FC, a direct comparison of these analysis methods has been lacking. As predicted based on comparisons of functional cortical networks (Rosazza et al., 2012) and from DTI work comparing seed-based analysis and ICA (O'Muircheartaigh et al., 2011), we largely identified analogous thalamic subdivisions between analysis techniques. However, variations in spatial specificity are highlighted, particularly in terms of the 'Somatosensory' ROI, which may reflect inherent methodological differences. For example, seed-based analysis is restricted to the pre-defined cortical ROIs, which in the current and previous work (Zhang et al., 2008) were large cortical subdivisions. This coarse

parcellation was designed to identify the primary thalamic subdivisions, while a more refined cortical parcellation could be applied to probe the thalamic sub-structure in more detail. Further, the seed-based approach using partial correlation, particularly when visualised using the WTA maps, assumes that thalamic regions are connected to single cortical areas. Even for first-order sensory nuclei, this is unlikely to be strictly true, as feedback connections from higher cortical areas act as modulators of the thalamic gate (Alitto and Usrey, 2003; Sherman, 2007; Sherman and Guillery, 1998, 2013). One advantage of ICA applied solely to thalamic voxels is that it identifies coherent subunits independently of their cortical connectivity, which potentially facilitates the identification of thalamic regions with widespread cortical connectivity. In addition, constraining the GICA to the thalamic ROI, meant that it was effectively a thalamic ROI selection method, and was therefore more likely to divide the thalamus into contiguous clusters. While selection of the appropriate dimensionality for the ICA decomposition is always an issue, the comparability of our results for 10 and 20 components suggests a degree of robustness against this choice.

Dice's coefficient allowed us to objectively quantify the spatial correspondence between group-level maps for the two analysis techniques (Figure 7) to uncover subtle differences between the seed-based and GICA maps. At least one GICA component displayed high spatial overlap with each of the seed-based maps, except for the 'Somatosensory' seed-based map. This lack of agreement for the 'Somatosensory' map is comparable to the seed-based FC results of small spatial extent of voxels correlated with the 'Somatosensory' seed ROI (Figure 2). Only three components had high Dice's coefficients with a single seed-based map, whilst other components were found to cover regions identified in multiple seed-based maps, which may be attributable to differences in spatial focus of either map (see section 3.1.3. for more details). Together, these findings imply that thalamocortical functional networks are complex, incorporating contributions from both multiple thalamic nuclei and diverse cortical regions. This view is supported by the existing electrophysiological literature, and such relationships potentially enable the thalamus to be a key integrative region in information processing pathways (Sherman, 2007; Sherman and Guillery, 2002, 2013).

Evaluating the GICA WTA maps and comparing them with the seed-based WTA maps provides further insight into the similarities of thalamic segmentation results from the two analyses. WTA approaches have been used in earlier works to condense structural (Behrens et al., 2003a; Johansen-Berg et al., 2005; Zhang et al., 2010) and functional (Kim et al., 2013; Zhang et al., 2008) thalamocortical connections. Here, the WTA approach was applied to assign each IC (and for the group-level and individual seed-based analyses each voxel) to a cortical ROI based upon maximal temporal correlation, and in so doing assessing the functional relevance of each IC (or voxel). While WTA maps provide a clear method to condense the rich dataset, they are based on only one aspect of the data (connectivity strength) and do not consider other aspects (e.g. extent or consistency). Comparable WTA maps were generated for both GICA dimensionalities with spatially contiguous components found to be correlated with the same ROI, thereby resulting in a map of discrete thalamic areas associated with each cortical ROI (Figure 6B). Regions of the thalamus found to be maximally correlated with the 'Prefrontal', 'Temporal' and 'Occipital and Parietal' ROIs were largely in agreement with equivalent group-level WTA maps from the seed-based analysis (Figure 6A). Conversely, the GICA WTA maps showed a much more extensive region connected with the 'Somatosensory' ROI, in contrast to the seed-based WTA results; a finding which is echoed by results from the computation of Dice's coefficient.

4.3. Comparison between present functional parcellations and those from previous work

Whilst the application and comparison of both seed-based FC analysis and GICA to evaluate thalamocortical connectivity is novel, these methodologies have been considered separately in the respective works of Zhang et al. (2008, 2010) and Kim et al. (2013). Although the functional parcellations presented here echo those from the literature, they do not show a direct correspondence, which may be the result of subtle methodological differences.

All three studies were performed on 3T MR scanners with equivalent acquisition parameters and included data from similarly sized cohorts. Resting state functional connectivity was evaluated in all studies; however, it is interesting to note that in the work of Zhang et al. (2008, 2010) participants

were asked to maintain visual fixation, in Kim et al. (2013) subjects' eyes were closed, and in the current study participants' eyes were open but not fixated. Fox et al. (2005) considered the effect of different resting state conditions (fixation, eyes open and eyes closed) on default mode and attention network connectivity and reported no difference, although work looking specifically at FC between the cortex and thalamus has suggested that eyes open vs. eyes closed may alter patterns of FC (Zou et al., 2009).

In terms of the preprocessing steps applied to the fMRI data our study largely employed the same as Zhang et al. and Kim et al. Preprocessing pipelines included the regression of nuisance variables from white matter and CSF signals (as well as movement parameters in Zhang et al. and this work). Zhang and colleagues did not apply any spatial smoothing, in contrast to Kim and colleagues who employed an 8mm FWHM kernel. In this work comparing both methods we applied a small spatial smoothing kernel (4mm FWHM) as a compromise between the two approaches. Furthermore, we have also replicated our seed-based results on data without spatial smoothing (Figure S2) and found that the smoothing we applied seemed to have little effect on the parcellation. In their supplementary analyses Kim et al. showed that the degree of smoothing can affect the ICA thalamic decomposition, but go on to acknowledge that the optimal level of smoothing is unclear. Whilst smoothing differences may have contributed a little to the variation between our GICA parcellations and those of Kim and colleagues, the large disparity in ICA dimensionality is likely to have had more of an impact.

Kim et al. performed a two-level ICA implemented in the GIFT ICA toolbox (http://mialab.mrn.org/software/gift/index.html). The first-level ICA was used to decompose wholebrain data into 50 components of which 3 were selected which covered the basal ganglia and thalamus. By combining these components and the AAL atlas, a subcortical ROI was selected and data from this subregion entered into the second-level ICA, which is akin to our GICA decompositions. From the 50 components outputted from this GICA Kim et al. highlighted 31 components that covered spatially distinct regions of the thalamus and basal ganglia. Using a

different back-projection method (Calhoun et al., 2009) to that implemented in this study, Kim et al. (2013) reported fairly consistent inter-subject localisation of thalamic components. Similar to these findings our 10 and 20 component ICA maps displayed physiologically plausible thalamic components which demonstrated quantitative overlaps with some of the same spatially distinct nuclei. A notable difference however between the two studies is that a majority of the components in Kim et al. were lateralized whilst ours were mainly bilateral (Figures 3 and 4). The number of lateralized components increased from our 10 to 20 component decompositions, suggesting that increased ICA dimensionality is responsible for the increased proportion of lateralized components observed by Kim and colleagues. The issue of ICA dimensionality is further discussed in section 4.7.

In comparison to Zhang et al. (2008) our seed-based results show more variation. For each of their cortical ROIs Zhang and colleagues reported group-level positive partial correlation maps covering bilateral, symmetric regions of the thalamus. Whilst our group-level seed-based maps (Figure 2) showed high partial correlation between equivalent cortical regions and a number of the same thalamic areas, our 'Somatosensory' ROI showed very little correlation with the thalamus at the group-level and our correlation maps were found to be less symmetric (e.g. the 'Occipital and Parietal' map) and patterns of correlation were seen to extend over areas of the thalamus thought to structurally project to different cortical regions. One methodological source of variability is the cortical ROI definition, which Zhang et al. defined via manual parcellation and therefore might not correspond exactly with ours. Whilst this difference could be further exaggerated by differing normalisation strategies, our cortical ROIs appear to be in agreement with theirs and given their extensive size the inclusion or exclusion of BOLD timecourses from a few voxels would be unlikely to significantly impact average seed timecourses. For our analyses FC was estimated over a continuous 15 minute acquisition, whereas Zhang and colleagues acquired a total of 28 minutes of resting state data per participant (over 4 separate runs). Whilst it is commonly assumed in the computation of static FC that connectivity is consistent over timescales such as these, their inclusion of nearly twice as much data could have acted to reduce 'noise' or variability in FC estimates. An additional potentially important difference between our analyses and those of Zhang et al. is that we focused

on correlations between the cortical ROIs and thalamus, whereas they computed wholehead partial correlation maps. They then focused on the thalamus by means of a fixed-effects approach, in contrast to the current random-effects procedures.

Despite some variability, our results largely support of those of Zhang et al. (2008, 2010) and Kim et al. (2013) and provide more evidence in this important area of investigation.

4.4. Comparison of group-level seed-based analysis and ICA results with histology

To date the identification of thalamic nuclei, for example when targeting specific nuclei for DBS, remains heavily reliant on the use of stereotactic thalamic atlases. In this work, we computed the overlap (assessed by computing Dice's coefficient) between our non-invasive functionally defined thalamic segmentations with a current "gold-standard", histologically defined thalamic atlas (Figure 8). In general, we observed higher spatial correspondence between GICA results and atlas nuclei, than for the seed-based maps. Whilst agreement between histology and the 'Temporal' seed-based map is apparent, correspondence with other seed-based maps was less clear. Except for the 'Somatosensory' seed-based map, which did not overlap with the expected thalamic nuclei, the remaining seed-based maps overlapped with expected atlas nuclei, but also more broadly with additional thalamic structures, which is not wholly unexpected given the sizeable cortical ROIs used for the seed-based analysis. Meanwhile, for the GICA results, high Dice's coefficients were measured between a number of components and single thalamic nuclei or subgroups of nuclei which have a common anatomical link with a particular part of the cortex (especially apparent for nuclei which connect to auditory and prefrontal cortices) (see section 3.1.4.). Similarly to the seed-based results, no components exclusively overlapped with nuclei which are believed to be maximally connected to somatosensory cortex.

The Dice's coefficient results imply that GICA yields a thalamic parcellation scheme with better correspondence to the histological "gold-standard" than the seed-based method, and further that GICA is better able to identify single thalamic nuclei or functional subgroups of nuclei. It should be noted, however, that neither methodology revealed a clearly separate region which overlapped with

ventral posterior nuclei and that whilst higher correlation coefficients were seen for the GICA, the maximum overlap with the atlas nuclei was found to be low, at approximately half of the values of overlap measured between the two functional parcellations. Low Dice coefficient values can be the result of a low number of voxels common to both images and/or because of a large difference in volumes between images, which cannot be resolved from the final generalized overlap value. To further clarify these overlap values, tables presenting the breakdown of generalized Dice coefficients are included (Tables S1, S2, S3, S4 and S5). When comparing the functional parcellations with the histological results, it is evident that for most GICA components and many seed-based maps, whilst overlap between them and the Morel atlas is low, the number of voxels in the functional parcellations is also much larger compared with images of the histological nuclei. This suggests that the spatial specificity of thalamocortical connections contained in the atlas has not been achieved with either functional segmentation. Whilst different methodological choices (e.g. regression of the global brain signal) may slightly alter the connectivity patterns (Fox et al., 2009), the inherently coarser spatial resolution of fMRI data in the current study (3x3x4 mm^3) compared with the digital stereotactic atlas (1 mm isotropic) may in part explain this discrepancy.

Conversely, it is not necessarily expected that there will be a direct one-to-one mapping between patterns of cytoarchitectural differences across the thalamus and their functional or structural MRI relationships with regions of the cortex. Future work will be needed to uncover the relationship between cytoarchitecture and MRI-based measures.

4.5. Comparison of group-level seed-based analysis and ICA results with structural connectivity

The DTI-defined Oxford thalamic atlas (Behrens et al., 2003a, 2003b) is frequently used to define parcellations of the thalamus in MRI studies. Previous work, mostly limited to cortical connectivity, has emphasised that whilst measures of FC and SC derived from MRI are complementary (Greicius et al., 2009; Hagmann et al., 2008; Hagmann et al., 2007; Honey et al., 2007; Johansen-Berg et al., 2004; Johnston et al., 2008; Khalsa et al., 2014; Mars et al., 2011; van den Heuvel et al., 2009; Zhang et al., 2010), they reveal distinct features of thalamocortical connectivity (Zhang et al., 2010). In this

work, by quantitatively comparing our functional parcellations with this atlas, we have been able to gain further insight into the similarities and differences between functionally- and structurally-defined thalamocortical connectivity patterns.

Whilst our results demonstrate some similarities between the seed-based and GICA results and the Oxford thalamic atlas segmentations, neither functional parcellation showed direct correspondence with the Oxford thalamic atlas, and additionally, differences in the patterns of agreement were also observed between the two functional methods. Employing Dice's coefficient, we found that some seed-based maps overlapped with Oxford atlas maps of regions with structural connections to the same cortical areas, whilst others overlapped with maps connected to different cortical areas ('Temporal') or showed diffuse overlap ('Somatosensory'). Meanwhile, for the GICA results some components demonstrated maximal overlap with a single Oxford atlas map (those connected to Occipital and Parietal cortices, Prefrontal cortex and Temporal lobe), implying that these components reflect the same thalamic regions as those from SC analyses. However, multiple components were found to show similar overlap values with the same Oxford atlas map and other components showed no specific overlap with any of the Oxford atlas maps. It should also be noted that neither seed-based or GICA results overlapped with the Oxford atlas map maximally connected to Somatosensory cortex.

Zhang and colleagues (2010) highlighted 'important differences' between their FC and SC defined thalamic maps (particularly in regions of the thalamus assigned to the Motor and Premotor and Prefrontal cortices), which they attributed to indirect polysynaptic connections (including connections between subcortical regions) which were not accounted for in the FC analysis and were not present in the SC analysis. Whilst our results differ from Zhang et al.'s in terms of the exact regions of the thalamus involved, (which could be the result of the differences observed between the seed-based results presented here and those presented in Zhang et al. (2008,2010)), our results support the claim from Zhang and colleagues that whilst FC and SC thalamocortical results are

complementary, caution is required when using a structurally-defined thalamic atlas to interpret functional data.

4.6. Assessing inter-subject spatial variability

In our final analyses, we used a WTA approach to evaluate the ability of the two analyses to study inter-individual variations in thalamic segmentation. Substantial variation in the spatial pattern of thalamocortical connectivity was observed across the group for both seed-based analysis and GICA (Figure 10A). Both analyses attributed the smallest percentage of thalamic voxels to the 'Somatosensory' ROI and on average the largest proportion of the thalamus was found to have the strongest connection with the 'Occipital and Parietal' ROI (Figure 10B and 10C). However, contrasting WTA structure was seen within participants across the two analyses. For the seed-based analysis, WTA assignment of thalamic voxels to the 'Occipital and Parietal' ROI was seen to dominate, whereas voxels for the GICA were more evenly assigned between the different cortical ROIs. Whilst the source of these observed differences between the functional parcellations remains unclear, certain methodological factors may be exacerbating them. For example, the WTA approach may be acting to enhance inter-individual FC differences by considering only a single feature of FC (connection strength). Other fundamentally-significant connections with other cortical ROIs are overlooked with this method. Additionally, in this work individual GICA WTA maps were generated following dual-regression as implemented in FSL. This is a validated technique for extracting individual subject components but methods such as independent vector analysis (IVA) (Michael et al., 2014) and back-projection as implemented in the GIFT ICA toolbox (Erdhardt et al., 2011) provide alternative frameworks.

The extent of the variation observed in the individual WTA maps is not in line with previous DTI work, which reported consistency across individual structural thalamic segmentations (Traynor et al., 2010). In agreement with this study however, Zhang et al. (2010) found that their functional parcellations across 3 participants were more variable than they predicted based on anatomy. Some of this unexpected variability might be attributable to DTI SC and BOLD FC measurements being

inherently sensitive to different aspects of inter-subject variability. DTI measures represent white matter tracts, whilst the nature of thalamocortical interactions represented in FC measures is less clear, but is likely to incorporate forward and backward connections between thalamus and other cortical regions, cortico-cortical connectivity, intra-thalamic connectivity and connectivity of both thalamus and cortex with other subcortical structures such as the striatum. Furthermore, FC is more sensitive to dynamic variation (Chang et al., 2010; Deco and Corbetta, 2013; Fox et al., 2005; Handwerker et al., 2012; Hutchinson et al., 2013a, 2013b; Liu et al., 2013; Wilson et al., 2015). To further investigate this important point, future study of effective connectivity may enable characterisation of the extent to which these variations affect inter-subject variability.

Furthermore, whilst some variability in size and arrangement of thalamic nuclei and thereby also functional thalamocortical networks is expected, the lack of an individual "gold-standard" makes it difficult to know which functional map is most reflective of true underlying individual variability. To date there has been very little work which has looked at the issue of inter-individual variability in the spatial arrangement and connectivity profile of thalamic nuclei (Burgel et al., 2006; Rademacher et al., 2002; Traynor et al., 2010). One way of addressing this would be to apply not only multiple different methods to functionally parcellate the thalamus in individual subjects as we have done, but to include other approaches in an attempt to reach a consensus parcellation. This could include structural MRI, such as those which have used T_1 and T_2 values (Deoni et al., 2005; Kanowski et al., 2014; Lenglet et al., 2012; Tourdias et al., 2014; Traynor et al., 2011), or parcellations based on tractography (Behrens et al., 2003a; Coenen et al., 2011; Johansen-Berg et al., 2005; Unrath et al., 2008; Wiegell et al., 2003; Zhang et al., 2010). Given the complementarities that have been identified when using structural and functional approaches to understand cortical organisation (Greicius et al., 2009; Hagmann et al., 2008; Hagmann et al., 2007; Honey et al., 2007; Johansen-Berg et al., 2004; Johnston et al., 2008; Khalsa et al., 2014; Mars et al., 2011; van den Heuvel et al., 2009), this could prove a fruitful line of investigation. One potential advantage of functional data is the potential estimation of the directionality of connections via the use of effective connectivity (Friston, 1994). This could be crucial in delineating modulator and driver connections (Sherman and Guillery,

1998) and thereby linking neuroimaging with invasive studies (discussed in more detail below). Comparison with the results of DBS associated with specific thalamic nuclei may also be a way of achieving some degree of validation, assuming that variability in the location of nuclei could be one of the reasons for variability in the success of DBS across individual patients (Caparros-Lefebvre et al., 1999; Luttjohann and van Luijtelaar, 2013). The methods we have applied, and the broader approaches that have been mentioned, could be used to address this question, providing a better understanding of the basic function and purpose of the thalamus in normal brain function, as well as more specific information about an individual thalamus for clinical applications such as DBS, and in relation to the variety of disorders mentioned in the Introduction in which thalamic involvement has been implicated.

4.7. Limitations and Future Work

In this work we employed seed-based analysis to evaluate functional relationships between five cortical regions and the thalamus. Despite the popularity and extensive use of the method for measuring FC, results from seed-based analysis are heavily dependent on the choice of the pre-defined ROI; as even small variations in the position of the seed can result in notable variations in FC patterns (Cole et al., 2010). We based our selection of *a priori* defined cortical ROIs on previous studies of both structural (Behrens et al., 2003a) and functional (Zhang et al., 2008) thalamocortical connectivity. Whilst the use of a more intricate parcellation of cortical areas would have generated different and possibly more detailed FC maps, we were restricted in our choice of ROIs since high correlations between timecourses from different cortical regions would result in unstable estimates of partial correlation (Zhang et al., 2008), and could have led to difficulties interpreting the numerous FC maps. Moreover, the question of how best to parcel the cortex into functionally relevant regions remains a prominent area of study in its own right (Craddock et al., 2012; Shirer et al., 2012; Yeo et al., 2011).

One way to avoid the need to specify pre-defined ROIs for FC analysis is to use ICA. However, in comparison with seed-based analysis ICA results can be less easy to interpret. ICA facilitates the

decomposition of MR data into a series of components, some of which reflect underlying neuronal fluctuations of interest, whilst others contain sources of noise or artifacts. The retention of components of interest is usually still performed based on subjective selection criteria (Calhoun et al., 2001; Calhoun et al., 2009; Kim et al., 2013; Malinen et al., 2007). Whilst, from visual inspection of the spatial maps, none of the components obviously represented noise, since we applied GICA to only a subregion of the brain, we were unable to infer which components represented noise based on comparison with previously reported patterns of artifactual components. Results from ICA can also be difficult to reproduce; firstly, within subjects due to the iterative algorithm which introduces run-to-run variability, and secondly due to altering the dimensionality of the ICA. The issue of ICA reliability can be addressed by implementing the ICASSO algorithm (Himberg et al., 2004), which is available when performing ICA using the GIFT ICA toolbox (http://mialab.mrn.org/software/gift/index.html). Here we ran GICA with dimensionalities of 10 and 20, which both revealed plausible and mainly bilateral thalamic subregions. Whilst thalamic parcellation results are largely in agreement with those from Kim et al. (2013), a prominent difference is that their 50 component GICA mainly extracted lateralised thalamic components, probably as a result of running GICA with a higher dimensionality. We tested the reproducibility of the bilaterality of our components by running GICA on separate thalamic hemispheres, which produced a set of lateralised components mirrored across hemispheres (Figure 5). It can be argued that there is no single 'best dimensionality', and moreover that the choice of dimensionality depends on the complexity of the question being asked of the data (Cole et al., 2010). Running ICA with a low dimensionality generally results in components representing "networks" of regions with related activity, whilst increasing the dimensionality acts to divide those regions across multiple components (Kiviniemi et al., 2003; Kiviniemi et al., 2009; Smith, 2012). The pattern of component splitting appears to be network specific. For instance, for moderate ICA dimensionalities, the left and right-hemispheric constituents of the central executive network are commonly split (White et al., 2010), while the anterior and posterior portions of the default mode network become dissociated (Starck et al., 2013). Our selection of relatively low dimensionalities was motivated by the belief that it is

unlikely that there would be a high number of truly independent functional subunits in the thalamus due to its size relative to our spatial resolution and by our interest to compare results with seed-based maps from a limited number of cortical regions.

Differences in spatial specificity between FC-defined thalamic subdivisions and the histological "gold-standard" thalamic atlas could be in-part addressed by acquiring fMRI data at higher magnetic field strength, e.g. 7T, which would facilitate improved spatial specificity of FC maps due to the afforded increases in signal-to-noise and spatial resolution. In addition, to better assess individual variations in thalamocortical connectivity patterns, future investigations of the thalamus would benefit from the identification of individually specific thalamic nuclei from anatomy which could then be used for comparison with FC and SC results. Promising advances are being made in this area using MRI relaxation time measures to achieve such contrast (Deoni et al., 2005; Traynor et al., 2011), particularly at 7T (Kanowski et al., 2014; Lenglet et al., 2012; Tourdias et al., 2014). However, as noted above, the relationship between the results obtained with different methodologies and modalities is not always clear.

Finally, while fMRI based techniques offer the opportunity to study the thalamus *in vivo*, they are inherently limited compared to invasive electrophysiological techniques in that the nature of the information being passed between regions is difficult to assess. This is particularly important to identify whether thalamocortical and corticothalamic connections are driving or modulating the signals being passed between regions. With the approaches we have taken, we cannot make inferences about the direction of information transfer. This could be addressed in future using metrics which assess effective connectivity (defined as the influence of one region over another, Friston, 1994), for example, dynamic causal modelling (DCM) (Friston et al., 2003) or lag-based methods such as Granger causality (Granger, 1969), however the use of haemodynamic signals to probe function at this level of detail is inherently challenging (Smith et al., 2011).

5. Conclusion

The use of both seed-based analysis and GICA to evaluate resting state fMRI data lead to plausible thalamic sub-structures being identified. Our findings at the group-level are in agreement with previous studies of thalamocortical connectivity and highlight the capability of using fMRI to inspect networks of cortical and subcortical structures. A general concordance between analyses is noted; however, direct comparison of seed-based and ICA thalamic segmentations revealed subtle differences in group-level and individual subject-level results. In the absence of individual-level ground truth parcellations which could unambiguously validate the results, convergence between methodologies and the natural emergence of bilateral regions is reassuring and suggests that the fMRI parcellations are neurobiologically meaningful. Further work will be needed to compare these functional parcellations with those based on structure, and to understand the behavioural effects of inter-individual variability in thalamic structure.

Acknowledgements:

This work was supported by the UK Engineering and Physical Sciences Research Council (grant number EP/J002909/1).

References

Alitto, H.J., Usrey, W.M., 2003. Corticothalamic feedback and sensory processing. Current Opinion in Neurobiology 13, 440-445.

Andreasen, N.C., 1997. The role of the thalamus in schizophrenia. Canadian Journal of Psychiatry-Revue Canadienne De Psychiatrie 42, 27-33.

Bagshaw, A.P., Rollings, D.T., Khalsa, S., Cavanna, A.E., 2014. Multimodal neuroimaging investigations of alterations to consciousness: The relationship between absence epilepsy and sleep. Epilepsy & Behavior 30, 33-37.

Baldassarre, A., Lewis, C.M., Committeri, G., Snyder, A.Z., Romani, G.L., Corbetta, M., 2012. Individual variability in functional connectivity predicts performance of a perceptual task. Proceedings of the National Academy of Sciences of the United States of America 109, 3516-3521.

Beckmann, C.F., DeLuca, M., Devlin, J.T., Smith, S.M., 2005. Investigations into resting-state connectivity using independent component analysis. Philosophical Transactions of the Royal Society B-Biological Sciences 360, 1001-1013.

Beckmann, C.F., Mackay, C.E., Filippini, N., Smith, S.A., 2009. Group comparison of resting-state fmri data using multi-subject ica and dual regression. 15th Annual Meeting of Organization for Human Brain Mapping poster 441 SU-AM.

Beckmann, C.F., Smith, S.A., 2004. Probabilistic independent component analysis for functional magnetic resonance imaging. Ieee Transactions on Medical Imaging 23, 137-152.

Behrens, T.E.J., Johansen-Berg, H., Woolrich, M.W., Smith, S.M., Wheeler-Kingshott, C.A.M., Boulby, P.A., Barker, G.J., Sillery, E.L., Sheehan, K., Ciccarelli, O., Thompson, A.J., Brady, J.M., Matthews, P.M., 2003a. Non-invasive mapping of connections between human thalamus and cortex using diffusion imaging. Nature Neuroscience 6, 750-757.

Behrens, T.E.J., Woolrich, M.W., Jenkinson, M., Johansen-Berg, H., Nunes, R.G., Clare, S., Matthews, P.M., Brady, J.M., Smith, S.M., 2003b. Characterization and propagation of uncertainty in diffusion-weighted MR imaging. Magnetic Resonance in Medicine 50, 1077-1088.

Birn, R.M., Diamond, J.B., Smith, M.A., Bandettini, P.A., 2006. Separating respiratory-variation-related fluctuations from neuronal-activity-related fluctuations in fMRI. NeuroImage 31, 1536-1548.

Biswal, B., Yetkin, F.Z., Haughton, V.M., Hyde, J.S., 1995. Functional connectivity in the motor cortex of resting human brain using echo-planar MRI. Magnetic Resonance in Medicine 34, 537-541.

Burgel, U., Amunts, K., Hoemke, L., Mohlberg, H., Gilsbach, J.M., Zilles, K., 2006. White matter fiber tracts of the human brain: Three-dimensional mapping at microscopic resolution, topography and intersubject variability. NeuroImage 29, 1092-1105.

Byne, W., Hazlett, E.A., Buchsbaum, M.S., Kemether, E., 2009. The thalamus and schizophrenia: current status of research. Acta Neuropathologica 117, 347-368.

Calhoun, V.D., Adali, T., McGinty, V.B., Pekar, J.J., Watson, T.D., Pearlson, G.D., 2001. fMRI activation in a visual-perception task: Network of areas detected using the general linear model and independent components analysis. NeuroImage 14, 1080-1088.

Calhoun, V.D., Liu, J., Adali, T., 2009. A review of group ICA for fMRI data and ICA for joint inference of imaging, genetic, and ERP data. NeuroImage 45, S163-S172.

Caparros-Lefebvre, D., Blond, S., Feltin, M.P., Pollak, P., Benabid, A.L., 1999. Improvement of levodopa induced dyskinesias by thalamic deep brain stimulation is related to slight variation in electrode placement: possible involvement of the centre median and parafascicularis complex. Journal of Neurology Neurosurgery and Psychiatry 67, 308-314.

Chang, C., Glover, G., (2010). Time–frequency dynamics of resting-state brain connectivity measured with fMRI. NeuroImage 50, 81-98.

Cifelli, A., Arridge, M., Jezzard, P., Esiri, M.M., Palace, J., Matthews, P.M., 2002. Thalamic neurodegeneration in multiple sclerosis. Annals of Neurology 52, 650-653.

Cole, D.M., Smith, S.M., Beckmann, C.F., 2010. Advances and pitfalls in the analysis and interpretation of resting-state FMRI data. Frontiers in systems neuroscience 4, 8-8.

Combarros, O., Miro, J., Berciano, J., 1994. Aguesia associated with thalamic plaque in multiple-sclerosis. European Neurology 34, 344-346.

Coenen, V.A., Allert, N., Mädler, B., 2011. A role of diffusion tensor imaging fiber tracking in deep brain stimulation surgery: DBS of the dentato-rubro-thalamic tract (drt) for the treatment of therapy-refractory tremor. Acta Neurochirurgica 153, 1579-1585.

Cordes, D., Haughton, V.M., Arfanakis, K., Wendt, G.J., Turski, P.A., Moritz, C.H., Quigley, M.A., Meyerand, M.E., 2000. Mapping functionally related regions of brain with functional connectivity MR imaging. American Journal of Neuroradiology 21, 1636-1644.

Craddock, R.C., James, G.A., Holtzheimer, P.E., III, Hu, X.P., Mayberg, H.S., 2012. A whole brain fMRI atlas generated via spatially constrained spectral clustering. Human Brain Mapping 33, 1914-1928.

Crum, W.R., Camara, O., Hill, D.L., 2006. Generalized overlap measures for evaluation and validation in medical image analysis. IEEE Transactions on Medical Imaging 25, 1451-1461.

De Luca, M., Beckmann, C.F., De Stefano, N., Matthews, P.M., Smith, S.M., 2006. fMRI resting state networks define distinct modes of long-distance interactions in the human brain. NeuroImage 29, 1359-1367.

Deco, G., Corbetta, M., The Dynamical Balance of the Brain at Rest. The Neuroscientist 17, 107-123.

Deoni, S.C.L., Josseau, M.J.C., Rutt, B.K., Peters, T.M., 2005. Visualization of thalamic nuclei on high resolution, multi-averaged T-1 and T-2 maps acquired at 1.5 T. Human Brain Mapping 25, 353-359.

Desikan, R.S., Segonne, F., Fischl, B., Quinn, B.T., Dickerson, B.C., Blacker, D., Buckner, R.L., Dale, A.M., Maguire, R.P., Hyman, B.T., Albert, M.S., Killiany, R.J., 2006. An automated labeling system for subdividing the human cerebral cortex on MRI scans into gyral based regions of interest. NeuroImage 31, 968-980.

Eidelberg, D., Galaburda, A.M., 1982. Symmetry and asymmetry in the human posterior thalamus. 1. Cytoarchitectonic analysis in normal persons Archives of Neurology 39, 325-332.

Erhardt, E. B., Rachakonda, S., Bedrick, E. J., Allen, E. A., Adali, T., Calhoun, V. D., 2011. Comparison of multi-subject ICA methods for analysis of fMRI data. Human Brain Mapping 32, 2075-2095.

Filippini, N., Macintosh, B., Goodwin, G., Frisoni, G., Smith, S.A., Matthews, P.M., Beckmann, C.F., Mackay, C.E., 2009. Distinct patterns of brain activity in young carriers of the APOE-epsilon4 allele. Proceedings of the National Academy of Sciences of the United States of America 106, 7209-7214.

Fisher, R.S., 2011. Direct brain stimulation is an effective therapy for epilepsy. Neurology 77, 1220-1221.

Fox, M.D., Raichle, M.E., 2007. Spontaneous fluctuations in brain activity observed with functional magnetic resonance imaging. Nature Reviews Neuroscience 8, 700-711.

Fox, M.D., Snyder, A.Z., Vincent, J.L., Corbetta, M., Van Essen, D.C., Raichle, M.E., 2005. The human brain is intrinsically organized into dynamic, anticorrelated functional networks. Proceedings of the National Academy of Sciences of the United States of America 102, 9673-9678.

Fox, M.D., Zhang, D., Snyder, A.Z., Raichle, M.E., 2009. The Global Signal and Observed Anticorrelated Resting State Brain Networks. Journal of Neurophysiology 101, 3270-3283.

Frazier, J.A., Chiu, S.F., Breeze, J.L., Makris, N., Lange, N., Kennedy, D.N., Herbert, M.R., Bent, E.K., Koneru, V.K., Dieterich, M.E., Hodge, S.M., Rauch, S.L., Grant, P.E., Cohen, B.M., Seidman, L.J., Caviness, V.S., Biederman, J., 2005. Structural brain magnetic resonance imaging of limbic and thalamic volumes in pediatric bipolar disorder. American Journal of Psychiatry 162, 1256-1265.

Friston, K.J., 1994. Functional and effective connectivity in neuroimaging: A synthesis. Human Brain Mapping 2, 56-78.

Friston, K.J., Harrison, L., Penny, W., 2003. Dynamic causal modelling. NeuroImage 19, 1273-1302.

Glover, G.H., Li, T.Q., Ress, D., 2000. Image-based method for retrospective correction of physiological motion effects in fMRI: RETROICOR. Magnetic Resonance in Medicine 44, 162-167.

Goldstein, J.M., Seidman, L.J., Makris, N., Ahern, T., O'Brien, L.M., Caviness, V.S., Jr., Kennedy, D.N., Faraone, S.V., Tsuang, M.T., 2007. Hypothalamic abnormalities in schizophrenia: Sex effects and genetic vulnerability. Biological Psychiatry 61, 935-945.

Granger, C.W.J., 1969. Investigating causal relations by econometric models and cross-spectral methods. Econometrica 37, 424-438.

Greicius, M.D., Krasnow, B., Reiss, A.L., Menon, V., 2003. Functional connectivity in the resting brain: A network analysis of the default mode hypothesis. Proceedings of the National Academy of Sciences of the United States of America 100, 253-258.

Greicius, M.D., Supekar, K., Menon, V., Dougherty, R.F., 2009. Resting-State Functional Connectivity Reflects Structural Connectivity in the Default Mode Network. Cerebral Cortex 19, 72-78.

Gusnard, D.A., Raichle, M.E., 2001. Searching for a baseline: Functional imaging and the resting human brain. Nature Reviews Neuroscience 2, 685-694.

Gustin, S.M., Peck, C.C., Wilcox, S.L., Nash, P.G., Murray, G.M., Henderson, L.A., 2011. Different Pain, Different Brain: Thalamic Anatomy in Neuropathic and Non-Neuropathic Chronic Pain Syndromes. Journal of Neuroscience 31, 5956-5964.

Hagmann, P., Cammoun, L., Gigandet, X., Meuli, R., Honey, C.J., Wedeen, V.J., Sporns, O., 2008. Mapping the structural core of human cerebral cortex. PLOS Biology 6, 1479-1493.

Hagmann, P., Kurant, M., Gigandet, X., Thiran, P., Wedeen, V.J., Meuli, R., Thiran, J.-P., 2007. Mapping Human Whole-Brain Structural Networks with Diffusion MRI. PLOS ONE 2.

Handwerker, D.A., Roopchansingh, V., Gonzalez-Castillo, J., Bandettini, P.A., 2012. Periodic changes in fMRI connectivity. NeuroImage 63, 1712-1719.

Henderson, J.M., Carpenter, K., Cartwright, H., Halliday, G.M., 2000. Loss of thalamic intralaminar nuclei in progressive supranuclear palsy and Parkinson's disease: clinical and therapeutic implications. Brain 123, 1410-1421.

Herrero, M.T., Barcia, C., Navarro, J.M., 2002. Functional anatomy of thalamus and basal ganglia. Childs Nervous System 18, 386-404.

Himberg, J., Hyvärinen, A., Esposito, F., 2004. Validating the independent components of neuroimaging time-series via clustering and visualization. NeuroImage 22, 1214-1222.

Honey, C.J., Koetter, R., Breakspear, M., Sporns, O., 2007. Network structure of cerebral cortex shapes functional connectivity on multiple time scales. Proceedings of the National Academy of Sciences of the United States of America 104, 10240-10245.

Honey, C.J., Sporns, O., Cammoun, L., Gigandet, X., Thiran, J.P., Meuli, R., Hagmann, P., 2009. Predicting human resting-state functional connectivity from structural connectivity. Proceedings of the National Academy of Sciences of the United States of America 106, 2035-2040.

Hubble, J.P., Busenbark, K.L., Wilkinson, S., Penn, R.D., Lyons, K., Koller, W.C., 1996. Deep brain stimulation for essential tremor. Neurology 46, 1150-1153.

Hutchinson, R.M., Womelsdorf, T., Gati, J.S., Everling, S., Menon, R.S., 2013b. Resting-State Networks Show Dynamic Functional Connectivity in Awake Humans and Anesthetized Macaques. Human Brain Mapping 34, 2154-2177.

Hutchinson, R.M., Womelsdorf, T., Allen, E.A., Bandettini, P.A., Calhoun, V.D., Corbetta, M., Penna, S.D., Duyn, J.H., Glover, G.H., Gonzalez-Castillo, J., Handwerker, D.A., Keilholz, S., Kiviniemi, V., Leopold, D.A., de Pasquale, F., Sporns, O., Walter, M., Chang, C., 2013b. Dynamic functional connectivity: Promise, issues, and interpretations. NeuroImage 80, 360-378.

Johansen-Berg, H., Behrens, T.E.J., Robson, M.D., Drobnjak, I., Rushworth, M.F.S., Brady, J.M., Smith, S.M., Higham, D.J., Matthews, P.M., 2004. Changes in connectivity profiles define functionally distinct regions in human medial frontal cortex. Proceedings of the National Academy of Sciences of the United States of America 101, 13335-13340.

Johansen-Berg, H., Behrens, T.E.J., Sillery, E., Ciccarelli, O., Thompson, A.J., Smith, S.M., Matthews, P.M., 2005. Functional-anatomical validation and individual variation of diffusion tractography-based segmentation of the human thalamus. Cerebral Cortex 15, 31-39.

Johnston, J.M., Vaishnavi, S.N., Smyth, M.D., Zhang, D., He, B.J., Zempel, J.M., Shimony, J.S., Snyder, A.Z., Raichle, M.E., 2008. Loss of resting interhemispheric functional connectivity after complete section of the corpus callosum. Journal of Neuroscience 28, 6453-6458.

Jones, E.G., 1998. Viewpoint: The core and matrix of thalamic organization. Neuroscience 85, 331-345.

Kanowski, M., Voges, J., Buentjen, L., Stadler, J., Heinze, H.J., Tempelmann, C., 2014. Direct visualization of anatomic subfields within the superior aspect of the human lateral thalamus by MRI at 7T. American Journal of Neuroradiology 35, 1721-7.

Khalsa, S., Mayhew, S., Chechlacz, M., Bagary, M., Bagshaw, A.P., 2014. The structural and functional connectivity of the posterior cingulate cortex: Comparison between deterministic and probabilistic tractography for the investigation of structure–function relationships. NeuroImage 102, 118-127.

Kim, D.-J., Park, B., Park, H.-J., 2013. Functional connectivity-based identification of subdivisions of the basal ganglia and thalamus using multilevel independent component analysis of resting state fMRI. Human Brain Mapping 34, 1371-1385.

Kiviniemi, V., Kantola, J.H., Jauhiainen, J., Hyvarinen, A., Tervonen, O., 2003. Independent component analysis of nondeterministic fMRI signal sources. NeuroImage 19, 253-260.

Kiviniemi, V., Starck, T., Remes, J., Long, X., Nikkinen, J., Haapea, M., Veijola, J., Moilanen, I., Isohanni, M., Zang, Y.-F., Tervonen, O., 2009. Functional Segmentation of the Brain Cortex Using High Model Order Group PICA. Human Brain Mapping 30, 3865-3886.

Klein, J., Hadar, R., Goetz, T., Maenner, A., Eberhardt, C., Baldassarri, J., Schmidt, T.T., Kupsch, A., Heinz, A., Morgenstern, R., Schneider, M., Weiner, I., Winter, C., 2013. Mapping Brain Regions in Which Deep Brain Stimulation Affects Schizophrenia-Like Behavior in Two Rat Models of Schizophrenia. Brain Stimulation 6, 490-499.

Koch, M.A., Norris, D.G., Hund-Georgiadis, M., 2002. An investigation of functional and anatomical connectivity using magnetic resonance imaging. NeuroImage 16, 241-250.

Krauth, A., Blanc, R., Poveda, A., Jeanmonod, D., Morel, A., Szekely, G., 2010. A mean three-dimensional atlas of the human thalamus: Generation from multiple histological data. NeuroImage 49, 2053-2062.

Krebs, C., Weinberg, J., Akesson, E., 2012. Neuroscience. Lippincott, Williams and Wilkins, Philadelphia, PA, USA.

Lenglet, C., Abosch, A., Yacoub, E., De Martino, F., Sapiro, Harel, N., 2012. Comprehensive in vivo Mapping of the Human Basal Ganglia and Thalamic Connectome in Individuals Using 7T MRI. PLOS ONE 7.

Llinas, R., 2003. Consciousness and the thalamocortical loop. International Congress Series 1250, 409-416.

Liu, X., Duyn, J.H., 2013. Time-varying functional network information extracted from brief instances of spontaneous brain activity. Proceedings of the National Academy of Sciences of the United States of America 110, 4392-4397.

Lowe, M.J., Mock, B.J., Sorenson, J.A., 1998. Functional connectivity in single and multislice echoplanar imaging using resting-state fluctuations. NeuroImage 7, 119-132.

Luttjohann, A., van Luijtelaar, G., 2013. Thalamic stimulation in absence epilepsy. Epilepsy Research 106, 136-145.

Mak, E., Bergsland, N., Dwyer, M.G., Zivadinov, R., Kandiah, N., 2014. Subcortical Atrophy Is Associated with Cognitive Impairment in Mild Parkinson Disease: A Combined Investigation of Volumetric Changes, Cortical Thickness, and Vertex-Based Shape Analysis. Am J Neuroradiol 35, 2257-2264.

Makris, N., Goldstein, J.M., Kennedy, D., Hodge, S.M., Caviness, V.S., Faraone, S.V., Tsuang, M.T., Seidman, L.J., 2006. Decreased volume of left and total anterior insular lobule in schizophrenia. Schizophrenia Research 83, 155-171.

Malinen, S., Hlushchuk, Y., Hari, R., 2007. Towards natural stimulation in MRI - Issues of data analysis. NeuroImage 35, 131-139.

Marrelec, G., Krainik, A., Duffau, H., Pelegrini-Issac, M., Lehericy, S., Doyon, J., Benali, H., 2006. Partial correlation for functional brain interactivity investigation in functional MRI. NeuroImage 32, 228-237.

Mars, R.B., Jbabdi, S., Sallet, J., O'Reilly, J.X., Croxson, P.L., Olivier, E., Noonan, M.P., Bergmann, C., Mitchell, A.S., Baxter, M.G., Behrens, T.E.J., Johansen-Berg, H., Tomassini, V., Miller, K.L., Rushworth, M.F.S., 2011. Diffusion-Weighted Imaging Tractography-Based Parcellation of the Human Parietal Cortex and Comparison with Human and Macaque Resting-State Functional Connectivity. Journal of Neuroscience 31, 4087-4100.

Michael, A.M., Anderson, M., Miller, R.L., Adalı, T., Calhoun, V.D., 2014. Preserving subject variability in group fMRI analysis: performance evaluation of GICA vs. IVA. Frontiers in Systems Neuroscience 8.

Morel, A., Magnin, M., Jeanmonod, D., 1997. Multiarchitectonic and stereotactic atlas of the human thalamus. Journal of Comparative Neurology 387, 588-630.

Mueller, S., Wang, D., Fox, M.D., Yeo, B.T.T., Sepulcre, J., Sabuncu, M.R., Shafee, R., Lu, J., Liu, H., 2013. Individual Variability in Functional Connectivity Architecture of the Human Brain. Neuron 77, 586-595.

Mumford, D., 1998. Thalamus. The handbook of brain theory and neural networks. MIT Press Cambridge, MA, USA, 981-984.

Murphy, K., Birn, R.M., Handwerker, D.A., Jones, T.B., Bandettini, P.A., 2009. The impact of global signal regression on resting state correlations: Are anti-correlated networks introduced? NeuroImage 44, 893-905.

Norden, A.D., Blumenfeld, H., 2002. The role of subcortical structures in human epilepsy. Epilepsy & Behavior 3, 219-231.

O'Muircheartaigh, J., Vollmar , C., Traynor, C., Barker, G.J., Kumari, V., Symms, M.R., Thompson, P., Duncan, J.S., Koepp, M.J., Richardson, M.P., 2011. Clustering probabilistic tractograms using independent component analysis applied to the thalamus. NeuroImage 54, 2020-2032.

Ooi, Y.C., Styliaras, J.C., Sharan, A., 2011. Thalamic Stimulation for Epilepsy. Neurosurgery Clinics of North America 22, 457-464.

Owen, S.L.F., Green, A.L., Stein, J.F., Aziz, T.Z., 2006. Deep brain stimulation for the alleviation of post-stroke neuropathic pain. Pain 120, 202-206.

Porta, M., Brambilla, A., Cavanna, A.E., Servello, D., Sassi, M., Rickards, H., Robertson, M.M., 2009. Thalamic deep brain stimulation for treatment-refractory Tourette syndrome Two-year outcome. Neurology 73, 1375-1380.

Putzke, J.D., Uitti, R.J., Obwegeser, A.A., Wszolek, Z.K., Wharen, R.E., 2005. Bilateral thalamic deep brain stimulation: midline tremor control. Journal of Neurology Neurosurgery and Psychiatry 76, 684-690.

Rademacher, J., Burgel, U., Zilles, K., 2002. Stereotaxic localization, intersubject variability, and interhemispheric differences of the human auditory thalamocortical system. NeuroImage 17, 142-160.

Raichle, M.E., MacLeod, A.M., Snyder, A.Z., Powers, W.J., Gusnard, D.A., Shulman, G.L., 2001. A default mode of brain function. Proceedings of the National Academy of Sciences of the United States of America 98, 676-682.

Rosazza, C., Minati, L., Ghielmetti, F., Mandelli, M.L., Bruzzone, M.G., 2012. Functional Connectivity during Resting-State Functional MR Imaging: Study of the Correspondence between Independent

Component Analysis and Region-of-Interest-Based Methods. American Journal of Neuroradiology 33, 180-187.

Saalmann, Y.B., 2014. Intralaminar and medial thalamic influence on cortical synchrony, information transmission and cognition. Frontiers in systems neuroscience 8, 83-83.

Serra, L., Cercignani, M., Carlesimo, G.A., Fadda, L., Tini, N., Giulietti, G., Caltagirone, C., Bozzali, M., 2013. Connectivity-Based Parcellation of the Thalamus Explains Specific Cognitive and Behavioural Symptoms in Patients with Bilateral Thalamic Infarct. PLOS ONE 8.

Sherman, S.M., 2007. The thalamus is more than just a relay. Current Opinion in Neurobiology 17, 417-422.

Sherman, S.M., Guillery, R.W., 1998. On the actions that one nerve cell can have on another: Distinguishing "drivers" from "modulators". Proceedings of the National Academy of Sciences of the United States of America 95, 7121-7126.

Sherman, S.M., Guillery, R.W., 2002. The role of the thalamus in the flow of information to the cortex. Philosophical Transactions of the Royal Society B-Biological Sciences 357, 1695-1708.

Sherman, S.M., Guillery, R.W., 2013. Functional connections of cortical areas MIT Press, Cambridge, MA, USA.

Shirer, W.R., Ryali, S., Rykhlevskaia, E., Menon, V., Greicius, M.D., 2012. Decoding Subject-Driven Cognitive States with Whole-Brain Connectivity Patterns. Cerebral Cortex 22, 158-165.

Smith, S.M., 2002. Fast robust automated brain extraction. Human Brain Mapping 17, 143-155.

Smith, S.M., 2012. The future of FMRI connectivity. NeuroImage 62, 1257-1266.

Smith, S.M., Fox, P.T., Miller, K.L., Glahn, D.C., Fox, P.M., Mackay, C.E., Filippini, N., Watkins, K.E., Toro, R., Laird, A.R., Beckmann, C.F., 2009. Correspondence of the brain's functional architecture during activation and rest. Proceedings of the National Academy of Sciences of the United States of America 106, 13040-13045.

Smith, S.M., Jenkinson, M., Woolrich, M.W., Beckmann, C.F., Behrens, T.E.J., Johansen-Berg, H., Bannister, P.R., De Luca, M., Drobnjak, I., Flitney, D.E., Niazy, R.K., Saunders, J., Vickers, J., Zhang, Y.Y., De Stefano, N., Brady, J.M., Matthews, P.M., 2004. Advances in functional and structural MR image analysis and implementation as FSL. NeuroImage 23, S208-S219.

Smith, S.M., Miller, K.L., Salimi-Khorshidi, G., Webster, M., Beckmann, C.F., Nichols, T.E., Ramsey, J.D., Woolrich, M.W., 2011. Network modelling methods for FMRI. NeuroImage 54, 875-891.

Starck, T., Nikkinen, J., Rahko, J., Remes, J., Hurtig, T., Haapsamo, H., Jussila, K., Kuusikko-Gauffin, S., Mattila, M.-L., Jansson-Verkasalo, E., Pauls, D.L., Ebeling, H., Moilanen, I., Tervonen, O., Kiviniemi, V.J., 2013. Resting state fMRI reveals a default mode dissociation between retrosplenial and medial prefrontal subnetworks in ASD despite motion scrubbing. Frontiers in Human Neuroscience 7.

Tourdias, T., Saranathan, M., Levesque, I.R., Su, J., Rutt, B.K., 2014. Visualization of intra-thalamic nuclei with optimized white-matter-nulled MPRAGE at 7 T. NeuroImage 84, 534-545.

Traynor, C., Heckemann, R.A., Hammers, A., O'Muircheartaigh, J., Crum, W.R., Barker, G.J., Richardson, M.P., 2010. Reproducibility of thalamic segmentation based on probabilistic tractography. NeuroImage 52, 69-85.

Traynor, C.R., Barker, G.J., Crum, W.R., Williams, S.C.R., Richardson, M.P., 2011. Segmentation of the thalamus in MRI based on T1 and T2. NeuroImage 56, 939-950.

Unrath, A., Klose, U., Grodd, W., Ludolph, A.C., Kassubek, J., 2008. Directional colour encoding of the human thalamus by diffusion tensor imaging. Neuroscience Letters 434, 322-327.

van den Heuvel, M.P., Mandl, R.C.W., Kahn, R.S., Pol, H.E.H., 2009. Functionally Linked Resting-State Networks Reflect the Underlying Structural Connectivity Architecture of the Human Brain. Human Brain Mapping 30, 3127-3141.

Van Dijk, K.R.A., Hedden, T., Venkataraman, A., Evans, K.C., Lazar, S.W., Buckner, R.L., 2010. Intrinsic Functional Connectivity As a Tool For Human Connectomics: Theory, Properties, and Optimization. Journal of Neurophysiology 103, 297-321.

Vincent, J.L., Patel, G.H., Fox, M.D., Snyder, A.Z., Baker, J.T., Van Essen, D.C., Zempel, J.M., Snyder, L.H., Corbetta, M., Raichle, M.E., 2007. Intrinsic functional architecture in the anaesthetized monkey brain. Nature 447, 83-U84.

White, T.P., Joseph, V., Francis, S.T., Liddle, P.F., 2010. Aberrant salience network (bilateral insula and anterior cingulate cortex) connectivity during information processing in schizophrenia. Schizophrenia Research 123, 105-115.

Weissenbacher, A., Kasess, C., Gerstl, F., Lanzenberger, R., Moser, E., Windischberger, C., 2009. Correlations and anticorrelations in resting-state functional connectivity MRI: A quantitative comparison of preprocessing strategies. NeuroImage 47, 1408-1416.

Wiegell, M.R., Tuch, D.S., Larsson, H.B.W., Wedeen, V.J., 2003. Automatic segmentation of thalamic nuclei from diffusion tensor magnetic resonance imaging. NeuroImage 19, 391-401.

Wilson, R.S., Mayhew, S.D., Rollings, D.T., Goldstone, A., Przezdzik,I., Arvanitis, T.N., Bagshaw, A.P., 2015. Influence of Epoch Length on Measurement of Dynamic Functional Connectivity in Wakefulness and Behavioural Validation in Sleep. NeuroImage, *In press*.

Woodward, N.D., Karbasforoushan, H., Heckers, S., 2012. Thalamocortical Dysconnectivity in Schizophrenia. American Journal of Psychiatry 169, 1092-1099.

Yeo, B.T.T., Krienen, F.M., Sepulcre, J., Sabuncu, M.R., Lashkari, D., Hollinshead, M., Roffman, J.L., Smoller, J.W., Zoeller, L., Polimeni, J.R., Fischl, B., Liu, H., Buckner, R.L., 2011. The organization of the human cerebral cortex estimated by intrinsic functional connectivity. Journal of Neurophysiology 106, 1125-1165.

Zhang, D., Snyder, A.Z., Fox, M.D., Sansbury, M.W., Shimony, J.S., Raichle, M.E., 2008. Intrinsic functional relations between human cerebral cortex and thalamus. Journal of Neurophysiology 100, 1740-1748.

Zhang, D., Snyder, A.Z., Shimony, J.S., Fox, M.D., Raichle, M.E., 2010. Noninvasive Functional and Structural Connectivity Mapping of the Human Thalamocortical System. Cerebral Cortex 20, 1187-1194.

Zou,Q., Long, D., Zuo,X.,Yan, C., Zhu, C., Yang, Y., Liu, D., He, Y., Zang, Y., 2009. Functional connectivity between the thalamus and visual cortex under eyes closed and eyes open conditions: A resting-state fMRI study. Human Brain Mapping 30, 3066-3078.

Figure Captions

Figure 1. A) Cortical ROI masks B) Thalamus ROI mask. All masks are shown overlaid on the standard MNI brain.

Figure 2. Group-level partial correlation maps between each thalamic voxel and each of the cortical ROIs. Height and extent thresholds correspond to $p < 0.001$. Images are shown overlaid on the standard MNI brain and displayed according to radiological convention.

Figure 3. Group maps of 10 independent components (ICs), computed on data from the whole thalamus ROI. ICs are threshold corresponding to alternative hypothesis threshold of $P > 0.5$. Results are shown overlaid on the standard MNI brain.

Figure 4. Group maps of 20 ICs, computed on data from the whole thalamus ROI. ICs are threshold corresponding to alternative hypothesis threshold of $P > 0.5$. Results are shown overlaid on the standard MNI brain.

Figure 5. Group maps using 10 ICs, extracted from the left (red-yellow) and right (blue) hemispheres of the thalamus. ICs are threshold corresponding to alternative hypothesis threshold of $P > 0.5$.

Figure 6. Group-level winner-take all (WTA) maps showing A) voxels colour-coded based on maximal partial correlation coefficient with each of the 5 cortical ROIs and B) ICs colour-coded based on maximal partial correlation with each of the 5 cortical ROIs, for 10 ICs (top row) and 20 ICs (bottom row). Results are shown overlaid on the standard MNI brain.

Figure 7. Generalized Dice overlap coefficients measured between the 10 ICs and group-level seed-based connectivity maps for each of the 5 cortical ROIs. Note that the colour of the bars represents each of the different cortical ROIs.

Figure 8. A) Select regions of a histological thalamic atlas (Krauth et al., 2010; Morel et al., 1997) colour-coded to show known anatomical connections between the thalamus and cortex; B) Generalized Dice overlap coefficients measured between group-level seed-based connectivity maps and select Morel nuclei presented the composite map in A) and C) Generalized Dice overlap coefficients measured between GICA components and select Morel nuclei presented the composite map in A). Note colours of bars in B) and C) are consistent with the colour-coding of nuclei in A). (For a list of thalamic ROI abbreviation definitions see Table S1).

Figure 9. A) Oxford thalamic DTI-defined atlas (Behrens et al., 2003a, 2003b) colour-coded to show structural connections between the thalamus and cortex; B) Generalized Dice overlap coefficients measured between group-level seed-based connectivity maps and Oxford thalamic atlas maps connected to each of the five cortical areas and C) Generalized Dice overlap coefficients measured between GICA components and each of the Oxford thalamic atlas maps connected to each of the five cortical areas. Note colours of bars in B) and C) are consistent with the colour-coding of Oxford thalamic parcellations in A).

Figure 10. A) WTA maps for each participant generated from seed-based connectivity analysis (left) and GICA (right). Results for a single slice ($z=39$) are shown overlaid on the standard MNI brain. Each voxel in the case of the seed-based analysis, or component for the GICA, is colour-coded based on the cortical ROI to which it displayed the highest positive partial correlation; B) Group mean percentage of thalamic voxels in seed-based WTA maps assigned to each cortical ROI. C) Group mean percentage of thalamic voxels in GICA WTA maps assigned to each cortical ROI. Error bars represent standard error across participants.

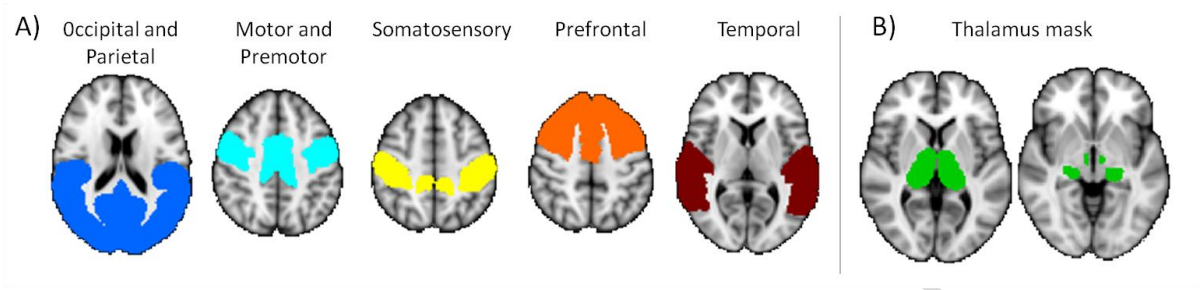

Fig. 1

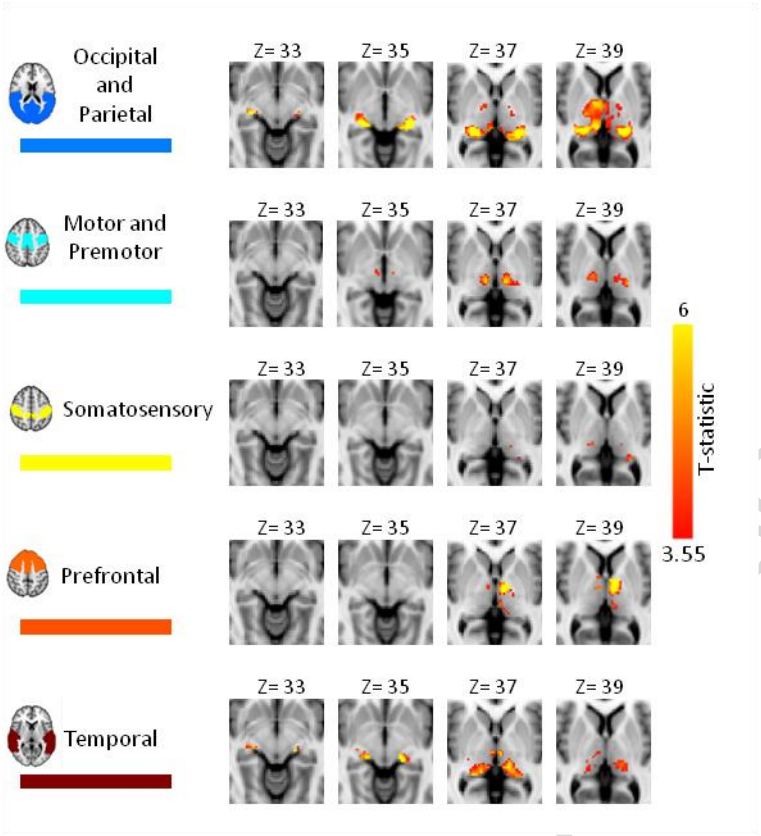

Fig. 2

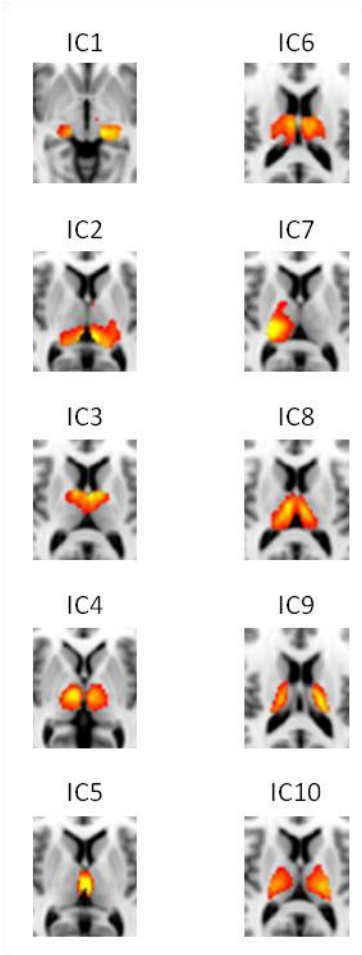

Fig. 3

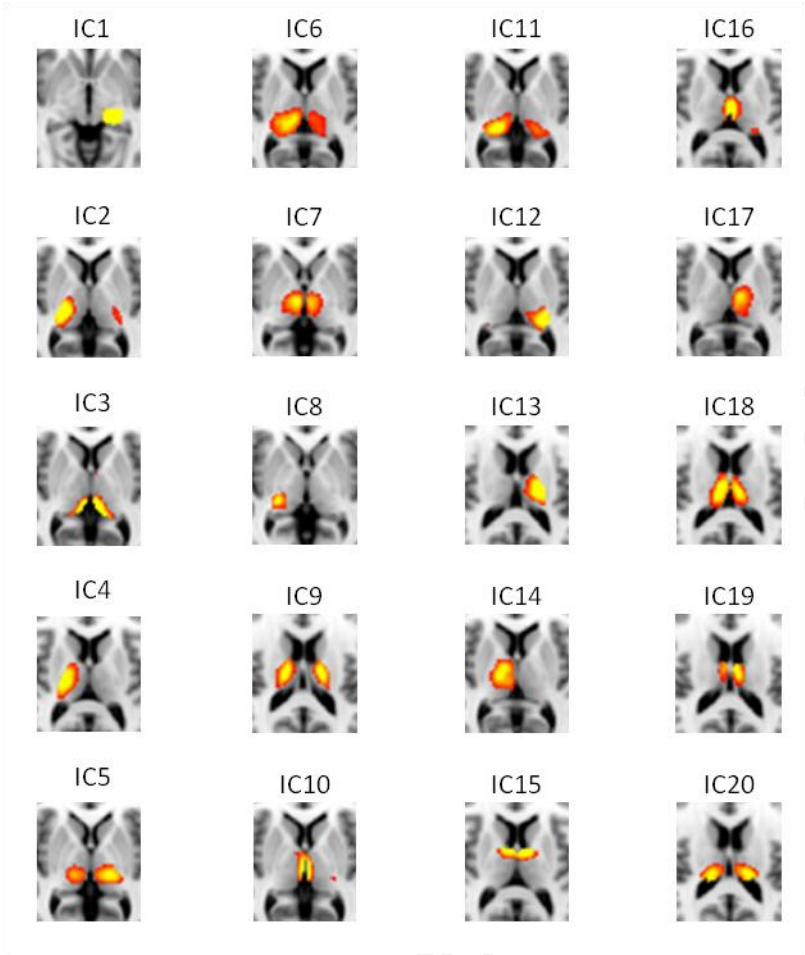

Fig. 4

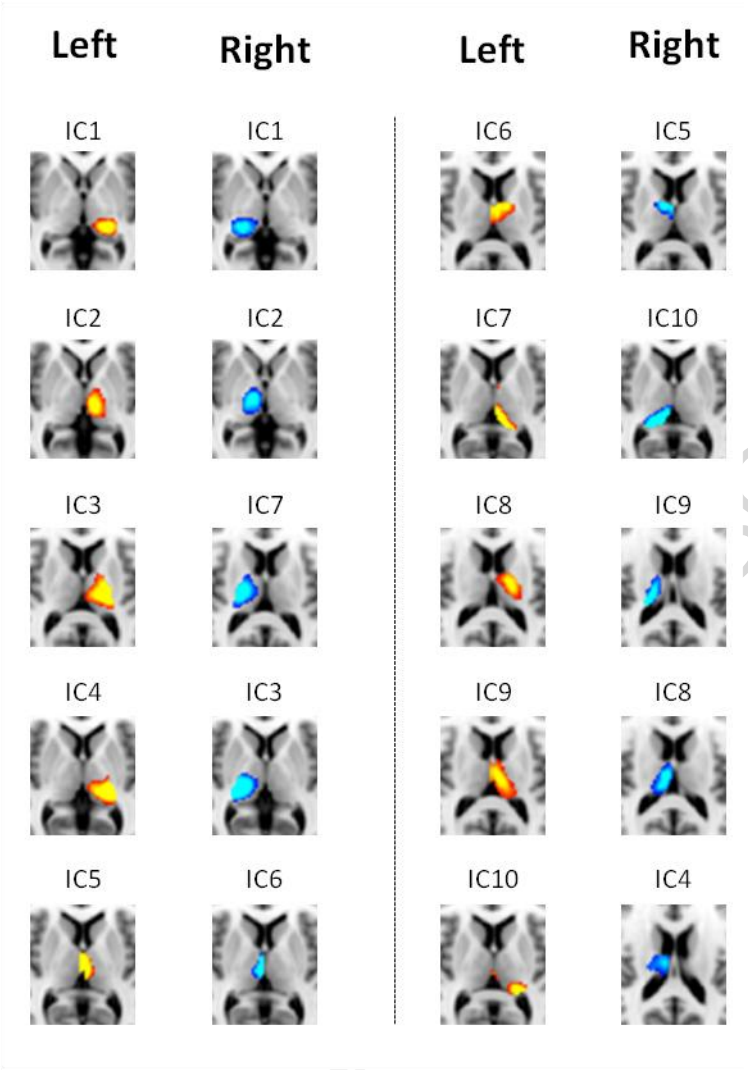

Fig. 5

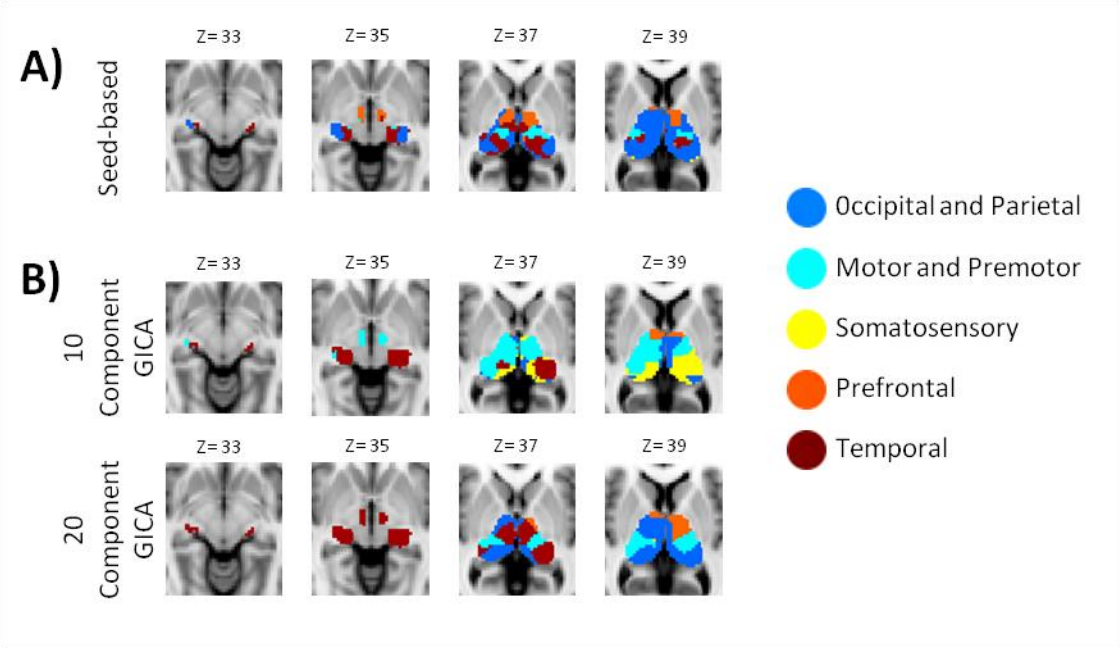

Fig. 6

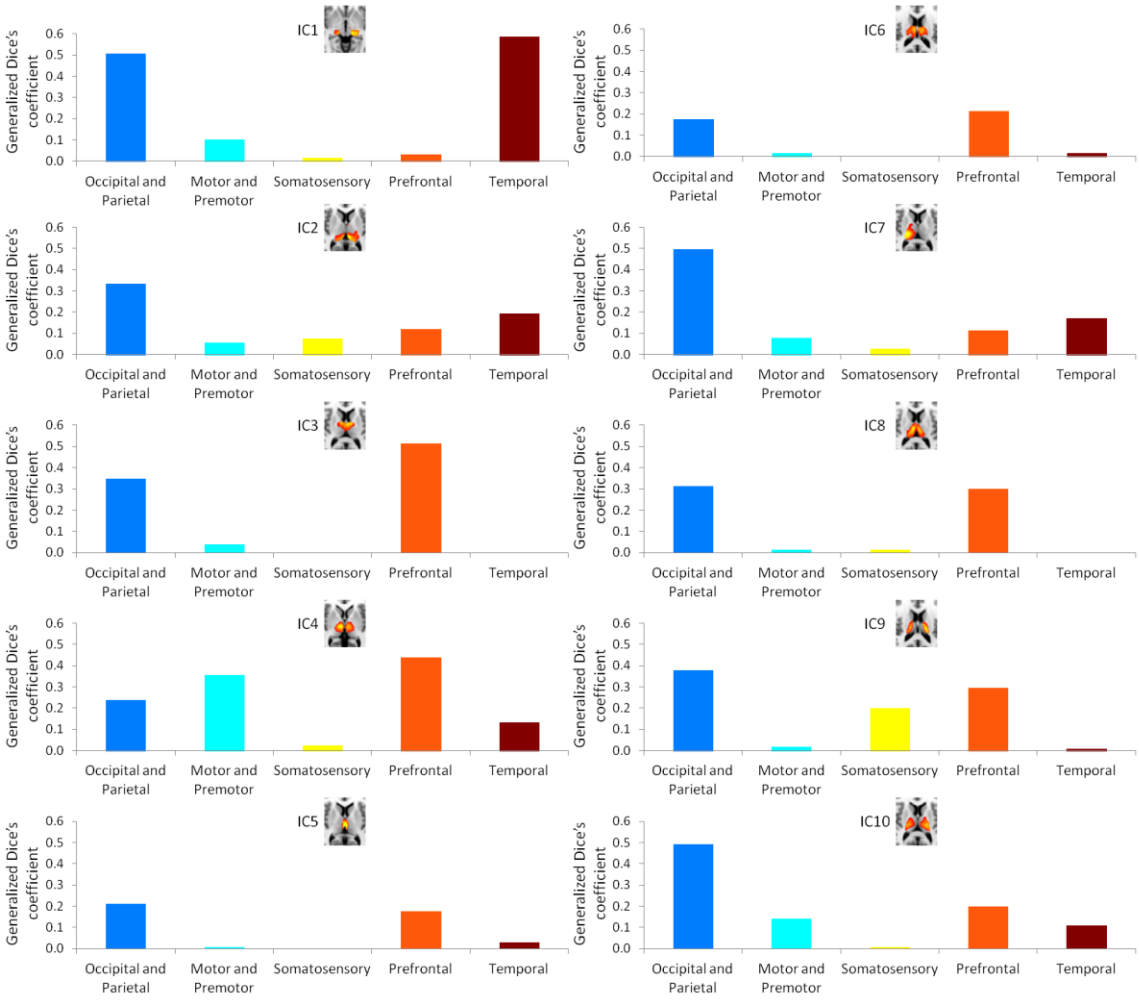

Fig. 7

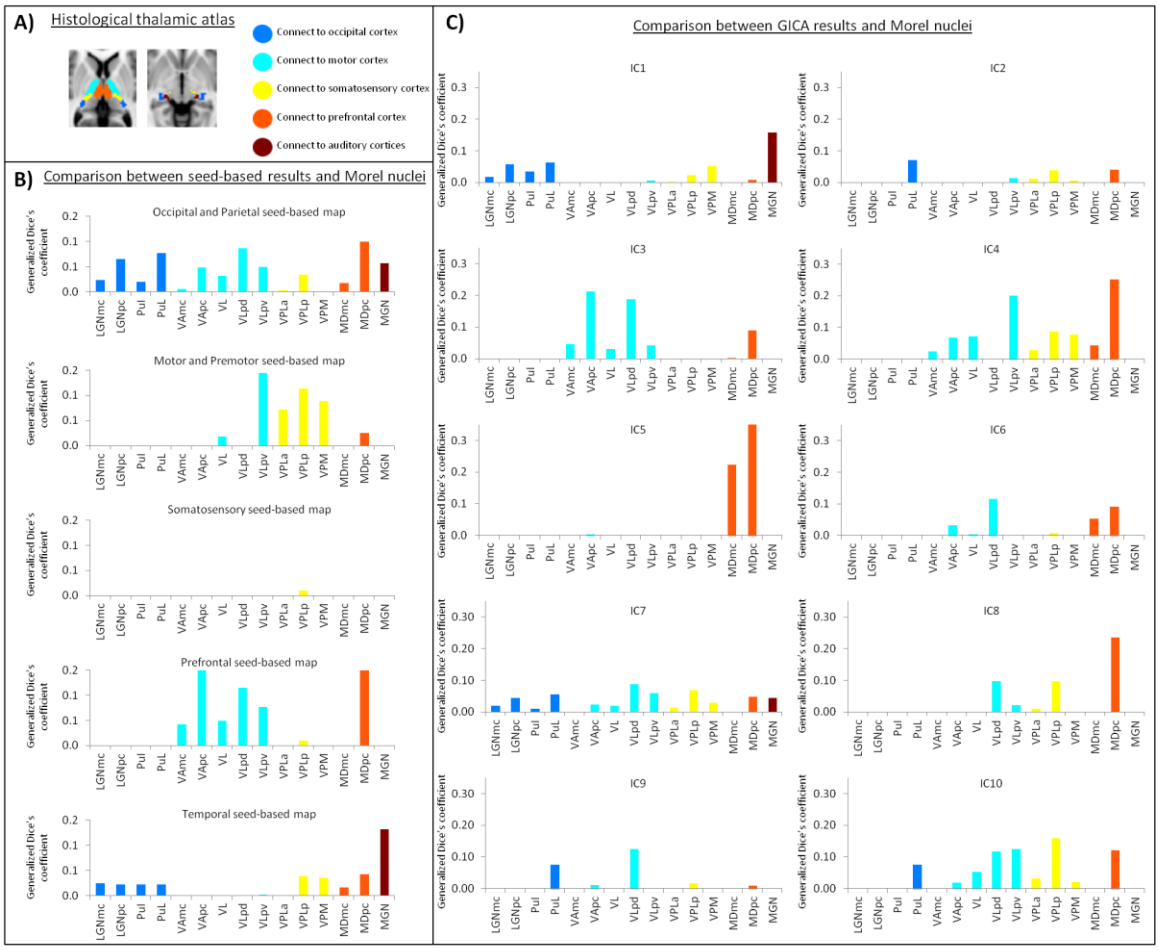

Fig. 8

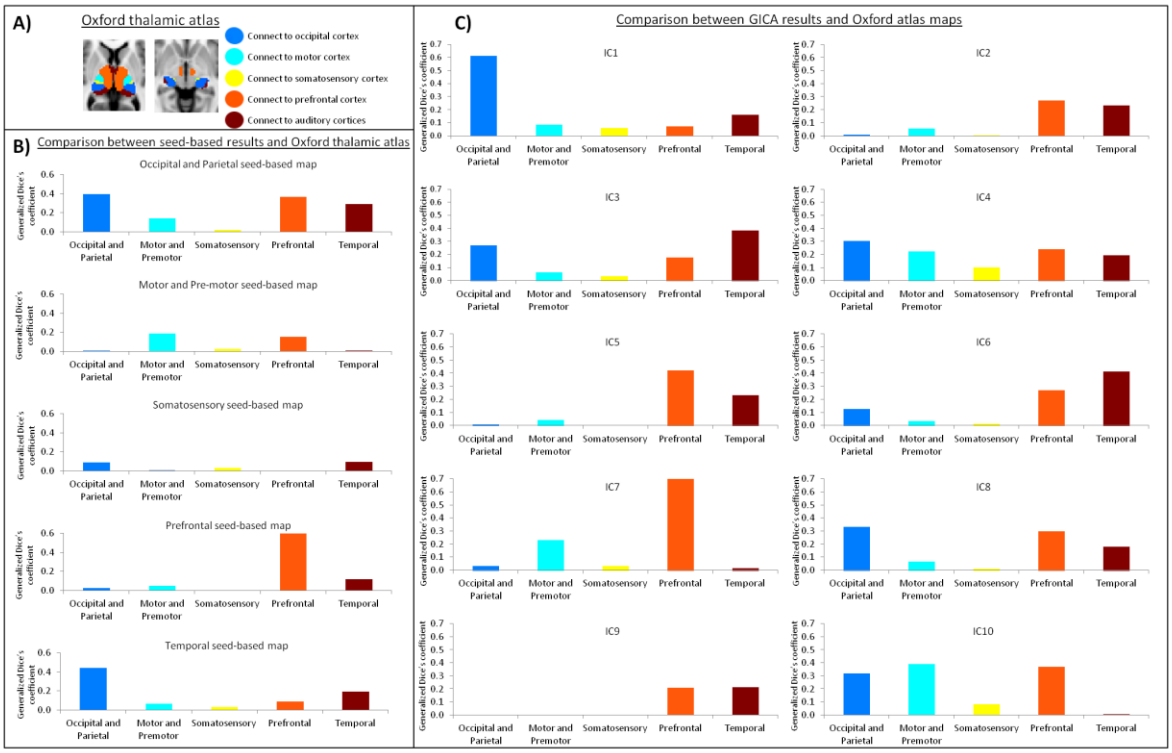

Fig. 9

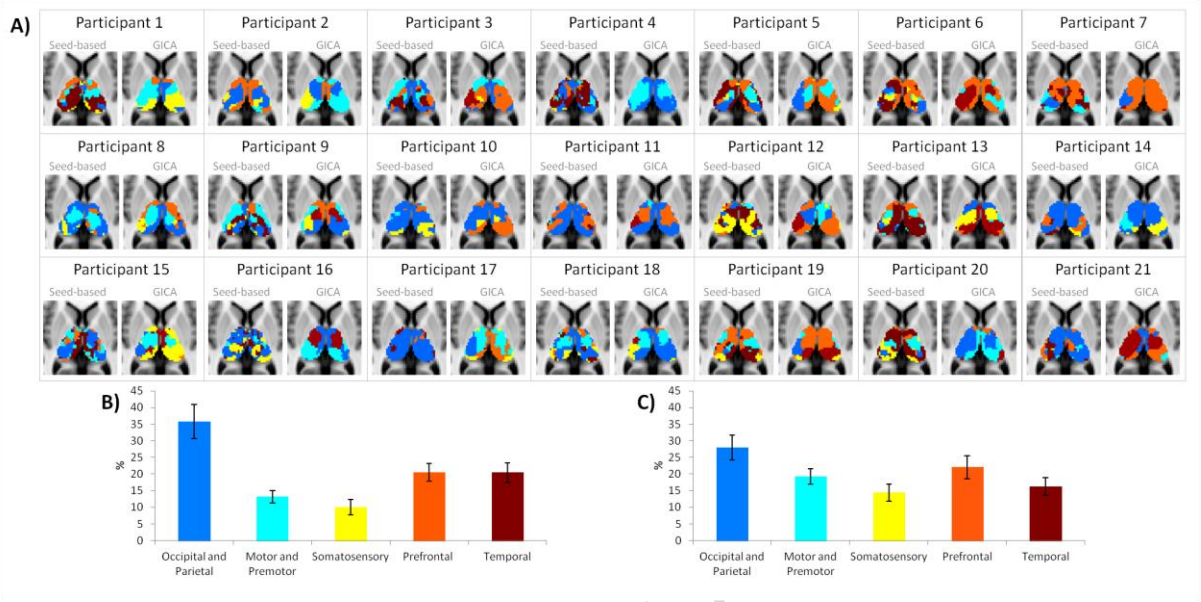

Fig. 10

RESEARCH HIGHLIGHTS

- Seed-based functional connectivity and ICA give plausible thalamic segmentations
- Subtle differences are found in group-level and individual subject-level results
- ICA provides additional specificity when comparing with a histological atlas
- Functional parcellations identify largely symmetrical bilateral regions
- Considerable inter-individual variability is observed with both methods